

TAILORING INTERFACIAL INTERACTIONS IN FIBER REINFORCED
POLYMERIC COMPOSITES BY THE ELECTROSPRAY DEPOSITION OF
WATERBORNE CARBON NANOTUBES

by
MURAT TANSAN

Submitted to the Graduate School of Engineering and Natural Sciences
in partial fulfillment of
the requirements for the degree of
Master of Science

SABANCI UNIVERSITY
MAY 2019

TAILORING INTERFACIAL INTERACTIONS IN FIBER REINFORCED
POLYMERIC COMPOSITES BY THE ELECTROSPRAY DEPOSITION OF
WATERBORNE CARBON NANOTUBES

APPROVED BY:

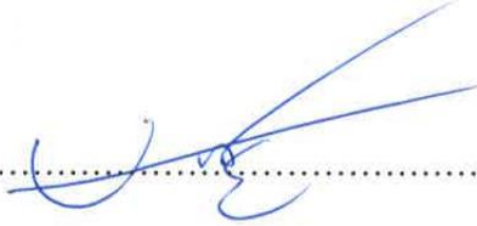
Asst. Prof. Serkan Ünal
(Thesis Supervisor)


.....

Prof. Dr. Mehmet Yıldız


.....

Assoc. Prof. Engin Burgaz


.....

© Murat Tansan 2019

All Rights Reserved

ABSTRACT

TAILORING INTERFACIAL INTERACTIONS IN FIBER REINFORCED POLYMERIC COMPOSITES BY THE ELECTROSPRAY DEPOSITION OF WATERBORNE CARBON NANOTUBES

MURAT TANSAN

Materials Science and Nano Engineering M.Sc. Thesis, May 2019

Thesis Supervisor: Assist. Prof. Serkan Ünal

Keywords: Electrospray, Carbon nanotubes, Carbon fiber reinforced polymeric composites, Vacuum infusion process, Fiber-matrix interface

The utilization of fiber reinforced polymeric composites (FRPCs) has been broadening in recent years, especially in aerospace, automobile and marine industries, sports goods and many other high-performance applications, all of which demand enhanced thermal, electrical and mechanical properties. The ultimate performance of FRPCs can be enhanced by improving the fiber-matrix interface. Using nanophase reinforcements; tailoring fiber-matrix interface with carbon nanotubes (CNTs) or other carbon nanomaterials has shown significant improvements in properties of the composite.

This thesis focuses on the deposition of CNTs onto carbon fabric (CF) surface by means of electrospray deposition and airbrush coating. Unlike the state-of-the-art methods to deposit carbon nanomaterials onto fiber surfaces, this study reports the deposition of CNTs from a waterborne dispersion, eliminates the use of organic volatile solvents and offers a method that is environmentally friendly and easily adaptable to large scale composite manufacturing processes. The hybrid CF-CNT structures prepared by surface deposition were used for the manufacturing of FPRCs by the vacuum infusion process

(VIP) to assess the influence of CNTs on the stress transfer between the fiber-matrix interface. The surface morphology of the hybrid CNT-CF structures was characterized using scanning electron microscopy to verify homogeneous dispersion of CNTs on CF fabrics. CNTs deliberately placed at the fiber-matrix interface are expected to serve as stress transfer bridges between the fiber and the matrix and contribute to the enhancement of interlaminar shear strength and flexural properties. As by measured Mode I and Mode II interlaminar fracture testing experiment, CNT deposition on the CF surface strengthens the attachment of the laminate plies.

ÖZET

FİBER TAKVİYELİ POLİMERİK KOMPOZİTLERİN ARA YÜZLERİNE ELEKTROSPREY KAPLAMA YÖNTEMİYLE SU BAZLI KARBON NANOTÜP EKLEME

MURAT TANSAN

Malzeme Bilimi ve Nano Mühendisliği, Yüksek Lisans Tezi, Mayıs 2019

Tez Danışmanı: Asist. Prof. Serkan Ünal

Anahtar Kelimeler: Karbon Nanotüp, Elektrosprey Kaplama, Karbon Elyaf Takviyeli
Polimerik Kompozitler, Vakum İnfüzyon, Fiber Reçine Ara yüzü

Elyaf takviyeli polimerik kompozitler (FRPC), üstün mekanik, termal, yapısal özellikler gösteren, korozyona dayanıklı, düşük öz kütleye sahip materyaller olup, bu özellikleri sayesinde havacılık endüstrisi, taşımacılık, inşaat ve denizcilik sektörlerinde yoğun şekilde kullanılmaktadırlar. Kompozit malzemelerin mekanik özellikleri, kullanım alanlarını ve kullanım sırasında sergiledikleri performansı doğrudan etkilemektedir. Yaşanan teknolojik gelişmelerle birlikte artan beklentiler neticesinde, kompozit malzemelerin daha yüksek mekanik özellikler sergilemeleri beklenmektedir. Literatürde, elyaf takviyeli polimerik kompozitlerin, kendisini oluşturan ana bileşenlerinin bazı nano uygulamalar ile takviye edilmesinin ardından mekanik, termal, elektriksel ve korozyon dayanımı özelliklerinin önemli ölçüde iyileştiğini gösteren pek çok çalışma mevcuttur.

Bu tez çalışmasında, elyaf takviyeli polimerik kompozitlerin fiber ile matris ara yüzünü iyileştirmeye yönelik olarak, elektrosprey metodu ve havalı boya tabancası yardımıyla spreyleme yöntemi ile su bazlı tek duvarlı karbon nanotüp dispersiyonu kompozit yapıya etkili bir şekilde entegre edilmiştir. Bu şekilde, ara yüze karbon nanotüplerin (CNT) verimli ve pratik bir şekilde entegrasyonunu sağlayarak, çevreye duyarlı bir metodun

geliştirilmesi, proses optimizasyon çalışmaları ile endüstride kullanılabilir hale getirilmesi hedeflenmiştir.

Karbon nanotüplerin kompozit yapıya etkili bir şekilde entegre edilmesi ve güçlendirme etkisi; elyaf ile polimer matrisin ara yüzeyindeki dağılımlarına ve konsantrasyonuna bağlıdır. Buna bağlı olarak karbon nanotüplerin elyaf üzerindeki morfolojileri elektron mikroskobu ile incelenmiştir. Elde edilen CNT-elyaf hibrit yapılar vakum infüzyon yöntemi ile FRPC üretiminde kullanılmıştır. Karbon nanotüplerin; kaplandıkları fiberin yüzey alanını arttırıp, polimer matrisin, elyaf ile olan ara yüzeyinde, aralarında bağlar kurulabilecek bölgeleri arttırarak, elyaftan reçineye etkili yük aktarımını güçlendirmeleri beklenmektedir.

Bu beklentiyi doğrulamak için üretilen numunelere uygulanan çeşitli mekanik testler sonucunda, mod-I ve mod-II kırılma tokluğu, katmanlar arası kayma mukavemeti ve eğme mukavemeti değerlerinde artış gözlenmiştir.

To my beloved companion, Odessa

ACKNOWLEDGEMENTS

I would first like to express my genuine gratitude and thanks to my supervisor Asst. Prof. Serkan Ünal for his immense patience, support and encouragement throughout my M.Sc. studies. With his guidance that I have been able to complete this project and it has been a privilege to be a part of his research group.

I would also like to thank my jury members, Prof. Dr. Mehmet Yıldız and Assoc. Prof. Engin Burgaz for dedicating their time and effort to give constructive reviews and support on this thesis.

The most special thanks and my sincere appreciation goes to Dr. Nuray Kızıldağ, M.Sc. Emine Billur Seviniş Özbulut, M.Sc. M.Sc. Ayşe Sayar Durmuş and M.Sc. Deniz Anıl. I was very lucky to have them by my side, helping and assisting me in every step of this research. Without their support and knowledge most of this work would not exist. I would also like to thank fellow members of the Unal group, M.Sc. Buket Taş, M.Sc. Erdiñ Taş, Necdet Özçelik, M.Sc. Ekin Berksun.

My colleagues and friends at Sabancı University Integrated Manufacturing Research and Application Center, İsa Emami Tabrizi, Dr. Çağatay Yılmaz, M.Sc. Çağdaş Akalın, Ertan Acar, M.Sc. Ragıp Orkun Seçer, Muhammed Enes Balkan, Sefa Kemal Mandal, M.Sc. Hilal Şenuysal and mechanical testing and materials characterization laboratory members also deserve special thanks. I am grateful for the help I received from them throughout this study.

I would be honored to thank my friends at Sabancı University; Onur Zırhlı, M.Sc. Yelda Yorulmaz, Melih Can Taşdelen, M.Sc. Farzin Javanshour. They have created the warmest office environment. M.Sc. Emre Burak Boz, M.Sc. Alp Ertunga Eyüpoğlu, joined me in this journey since high school for 12 years. I am delighted to thank to very close friends; Hazal Buluttekın, Pınar Boykurt, M.Sc. Ali Büyükoğlu, M.Sc. Mert Özer, Deniz Akural who have given me the motivation and made life happier with constant support. Also, thanks to my flat mates, Sarp Terlemez, Engin Us, Caner Etlı, İsmet Ata Erduran who were always backing me up.

Finally, I would like to express my deepest gratitude to my family for their endless love and encouragement throughout my whole life journey. Especially to my mother who was always there to help me even when it comes to preparing FRPC test specimens.

This project is supported by The Scientific and Technological Research Council of Turkey (TÜBİTAK) under the grant agreement number 215M116. Authors also acknowledge the support by the European Union Seventh Framework Programme (FP7/2007-2013) under grant agreement number PCIG12-GA-2012-334577.

TABLE OF CONTENTS

ABSTRACT	iv
ÖZET	vi
ACKNOWLEDGEMENTS	ix
TABLE OF CONTENTS	xi
LIST OF FIGURES	xiii
LIST OF TABLES	xv
LIST OF ABBREVIATIONS	xvi
Chapter 1 INTRODUCTION	1
1.1. Organization of the thesis	2
1.2. Carbon Nanotubes (CNTs)	2
1.2.1. Structure of CNTs	3
1.2.2. Properties of CNTs	3
1.2.3. Applications of CNTs	4
1.3. Integration of CNTs into Fiber Reinforced Polymeric Composites (FRPCs) 5	
Chapter 2 EXPERIMENTAL	8
2.1. Materials	8
2.2. Preparation of Waterborne SWCNT Dispersions	8
2.3. Spray Deposition of SWCNTs	9
2.3.1. Electrospray Deposition	9
2.3.2. Air Brush Spray Deposition	10
2.4. Manufacturing of SWCNT Incorporated FRPCs	11
2.4.1. Vacuum Infusion Process (VIP)	15
2.4.2. Specimen Preparation.....	17
2.5. Characterization	17
2.5.1. Thermogravimetric Analysis	17
2.5.1. Scanning Electron Microscopy (SEM)	17
2.5.2. Mechanical Testing of FRPC Materials	18

2.5.2.1. Tensile Test.....	18
2.5.2.2. Mode I Fracture Toughness Test	19
2.5.2.3. Mode II Fracture Toughness Test	20
2.5.2.4. Three Point Bending Test (Flexural test)	22
2.5.2.5. Short Beam Shear Test	22
2.5.2.6. V-Notched Shear Test	23
Chapter 3 RESULTS AND DISCUSSION	24
3.1. Characterization Results	24
3.1.1. Characterization of SWCNT Dispersions	24
3.1.2. Spray Deposition of SWCNTs	25
3.1.3. SEM Analysis of Sprayed CF Fabrics	30
3.2. Structural Characterization of FRPC Panels	34
3.3. Mechanical Characterization of FRPCs	36
3.3.1. Tensile Tests	36
3.3.2. Mode I Fracture Toughness Test Results	40
3.3.3. Mode II Fracture Toughness Test Results.....	43
3.3.4. Three-Point Bending Test Results	44
3.3.5. Short Beam Bending Test Results	49
3.3.6. V-Notched Shear Test Results.....	50
3.4. SEM Analysis of Fractured Surfaces	52
Chapter 4 CONCLUSIONS	54
REFERENCES	56

LIST OF FIGURES

Figure 2.1 Vacuum filtration setup for SWCNT-H ₂ O dispersions	9
Figure 2.2 In-house built electrospray deposition unit	10
Figure 2.3 (a), (b) and (c) shows airbrush setup, (d) airbrush with extended reservoir ..	11
Figure 2.4 VIP steps, (a) alignment of carbon fabrics, (b) PTFE tabs for fracture testing, (c) peel ply, (d) PTFE for easy removal of composites after curing, (e) flow mesh ensuring flow of resin	16
Figure 2.5 Bagging step in VIP.....	16
Figure 2.6 VIP steps; (a) vacuum gage, (b-c) resin flow under ambient pressure.....	16
Figure 2.7 (a-b) Thermal imaging of heat table, (c) isolator for VIP.....	17
Figure 2.8 Tensile test specimens with aluminum tabs bonded on both ends	18
Figure 2.9 Mode I fracture toughness test specimen [59]	19
Figure 2.10 Mode-I fracture toughness test setup.....	20
Figure 2.11 Mode II fracture toughness test specimen [60]	21
Figure 2.12 Mode-II fracture toughness test setup.....	21
Figure 2.13 Three-point bending test setup	22
Figure 2.14 Short beam shear test setup	23
Figure 2.15 V-notched test specimens	23
Figure 3.1 Determination of SWCNT concentrations by UV-Vis Spectroscopy after filtration.....	25
Figure 3.2 Schematic representation of electrospray	27
Figure 3.3 Positioning of crocodiles along syringe nozzles (Ideal positions #2,#4,#3)..	28
Figure 3.4 Effects of different crocodile positions along nozzles on the spraying	28
Figure 3.5 SEM images of airbrush sprayed 6 mg/m ² SWCNT on CF fabric; (a-b) 40Kx at 3kV.....	30
Figure 3.6 SEM images of 6 mg/m ² SWCNT electrosprayed on CF fabric at 13.5kV; (a) 40Kx at 3kV (b) 25Kx 3kV.....	31
Figure 3.7 SEM images of airbrush sprayed 12 mg/m ² SWCNT on CF fabric (a) 30Kx at 3kv (b) 20Kx at 3kV.....	31
Figure 3.8 SEM images of 12 mg/m ² SWCNT electrosprayed on CF fabric at 13.5kV; (a- b) 20Kx at 3kV	31
Figure 3.9 SEM images of 18 mg/m ² SWCNT electrosprayed on CF fabric at 13.5kV (a) 20Kx at 2kV (b-c) 50Kx at 2kV (d) 50Kx at 5kV.....	32

Figure 3.10 SEM images of airbrush sprayed 18 mg/m ² SWCNT on CF fabric (a,c) 20Kx at 3kv (b) 20Kx at 3kV (d) 100Kx at 3kV	32
Figure 3.11 SEM images of PVP only electro sprayed on CF fabric equivalent to 6 mg/m ² SWCNT deposition conditions at 13.5kV, (a) 5Kx at 3kV (b) 10Kx at 3kV	33
Figure 3.12 SEM images of PVP only electro sprayed on CF fabric equivalent to 12 mg/m ² SWCNT deposition conditions at 13.5kV (a) 5Kx at 3kV (b) 15Kx at 3kV	33
Figure 3.13 SEM images of PVP only electro sprayed CF fabric equivalent to 18 mg/m ² SWCNT deposition conditions at 13.5kV (a) 5Kx at 3kV (b) 10Kx at 3kV	33
Figure 3.14 Tensile stress versus strain curves of (a) AB1, (b) AB2 batches	37
Figure 3.15 Tensile stress versus strain curves of (a) ES1, (b) ES2 batches	38
Figure 3.16 Load versus tensile extension graph, Mode-I fracture toughness test of (a) ES1, (b) AB4 batches	41
Figure 3.17 Load versus tensile extension graph, Mode-I fracture toughness test of (a) ES2, (b) ES4 batches	42
Figure 3.18 Load versus flexure extension graph, Mode-II fracture toughness test of (a) ES2, (b) AB4 batches	44
Figure 3.19 Flexural Stress versus flexural strain of (a) AB1 and (b) AB2 batches.....	46
Figure 3.20 Flexural Stress versus flexural strain of (a) ES1 and (b) ES2 batches	46
Figure 3.21 Flexural Stress versus flexural strain of AB6 batch	47
Figure 3.22 Load versus flexural extension, ILSS of (a) ES2 and (b) AB6 batches	49
Figure 3.23 Compressive stress versus compressive strain graph of (a) ES1 and (b) ES2 batches obtained from V-notched method	51
Figure 3.24 Compressive stress versus compressive strain graph of AB6 batch obtained from V-notched method.....	52
Figure 3.25 SEM images of fractured mode-I specimen ES2_200 sample.....	52
Figure 3.26 SEM images of SWCNT matrix-fiber bridging in ES2_200 sample	53

LIST OF TABLES

Table 2.1 List of all manufactured composites	14
Table 2.1 List of all manufactured composites (continued)	15
Table 3.1 Comparison of airbrush and electro spray methods	29
Table 3.2 Properties of manufactured composites, average density, void content, fiber-resin ratio.....	34
Table 3.3 Tensile test results of airbrush sprayed AB1 batch	36
Table 3.4 Tensile test results of airbrush sprayed AB2 batch	37
Table 3.5 Tensile test results of electro sprayed ES1 batch	38
Table 3.6 Tensile test results of electro sprayed ES2 batch	39
Table 3.7 Tensile test results of airbrush sprayed or electro sprayed ES/AB batch	39
Table 3.8 Mode-I fracture toughness test results of ES1 batch	40
Table 3.9 Mode-I fracture toughness test results of AB4 batch	41
Table 3.10 Mode-I fracture toughness test results of ES2 batch	42
Table 3.11 Mode-I Fracture Toughness Test Results of ES4 Batch	43
Table 3.12 Mode-II Fracture Toughness Test Results of AB4 batch.....	43
Table 3.13 Mode-II Fracture Toughness Test Results of ES2 batch	44
Table 3.14 Three-point bending test results of AB1 batch.....	45
Table 3.15 Three-point bending test results of AB2 batch.....	45
Table 3.16. Three-point bending test results of ES1 batch.....	46
Table 3.17 Three-point bending test results of ES2 batch.....	47
Table 3.18 Three-point bending test results of AB6 batches.....	47
Table 3.19 Three-point bending test results of ES/AB batch	48
Table 3.20 Short beam shear test results of ES2 batch	49
Table 3.21 Short beam shear test results of AB6 batch.....	50
Table 3.22 Shear properties of ES1 batch	50
Table 3.23 Shear properties of ES2 batch	51
Table 3.24 Shear properties of AB6.....	51

LIST OF ABBREVIATIONS

FRPC: Fiber Reinforced Polymeric Composites

(MW/SW) CNT: (Multi Walled/Single Walled) Carbon Nanotube

CVD: Chemical Vapor Deposition

RTM: Resin Transfer Molding

VIP: Vacuum Infusion Process

DCB: Double Cantilever Beam

ENF: End-notched flexure

SEM: Scanning Electron Microscopy

DD: Dipping Deposition

PAN: Polyacrylonitrile

Chapter 1

INTRODUCTION

The practical application areas and remarkable intrinsic properties drive the growing interest in carbon nanotubes (CNTs) for use in various structural materials. Their potential use in composite materials, especially fiber reinforced polymeric composites (FRPCs) is particularly of interest, as CNTs possess extraordinary electrical and thermal properties, which can be valuable in improving polymer matrix properties, as well as fibers. Its improvements in the mechanical performance of matrices have been limited, likely due to the short supply of high quality, cost effective CNTs and difficulties in dispersing them in the matrix, as well as handling high loading fractions of CNTs and keeping a strong interfacial bond between resin and the fiber. It can still be used in a variety of practical ways, where conventional nano-reinforcements fail, specifically in fine structures like polymeric fibers, foams and films. Some promising results of using CNTs include improvements in electrical conductivity, thermal conductivity, wear resistance, service temperature, flame retardancy, surface finish and biological interactions [1,2].

The use of FRPCs over the past half-century have been numerous and profound. This is largely due to the combination of their high-caliber mechanical properties and low weight, as well as their abilities to withstand chemical and environmental threats. These attributes make them useful in a plethora of industries, namely sporting goods, aviation, automotive, the marine industry and civil engineering. The main drawbacks in FRPCs include comparatively weak compression and interlaminar interactions [3].

The weakest part of the FRPCs are the matrices, and CNTs can be added to enhance and overcome these existing limitations and challenges, which is the main motivation of this thesis. If they are incorporated into FRPCs properly, CNTs can offer benefits such as

intralaminar and interlaminar reinforcement, create additional damage processes to improve local toughness of a fractured matrix, improve fiber-surface area, create mechanical anchorage to intertwine the fiber and the matrix, and enhance stress transfer by additional bridging between the fiber and the matrix [4] .

1.1. Organization of the thesis

In Chapter 1, after providing introductory information about FRPCs, their developments in the course of time and future requirements for the need of enhancing their performance, CNTs are discussed as an ideal candidate for nano reinforcing material in FRPCs. Chapter 1 concludes with a brief discussion about the state-of-the-art CNT integration techniques into FRPCs. Chapter 2 gives the experimental studies on the route to integrate single walled carbon nanotubes (SWCNTs) into the FRPC structure from waterborne dispersions with the design and optimization of the SWCNT deposition and FRPC fabrication processes. Details of the samples preparation and characterization methods are also explained in this part. In Chapter 3, outcomes of mechanical tests, SEM images and other characterization techniques for all FRPC samples are discussed individually and comparatively to understand the effect of different deposition techniques and SWCNT content on the properties of FRPCs. In Chapter 4, main conclusions of this thesis are presented.

1.2. Carbon Nanotubes (CNTs)

The discovery of CNTs is attributed to Iijima in 1991 [5], however, in 1952 Radushkevich and Lukyanovich did the first observations of tubular carbon filament moieties having nanometer size diameter [6]. It was unfortunate that, the graphitic structure in the nanotube walls weren't distinguished well with resolution of TEM at that time [3]. After 1991, Iijima successfully observed CNT structures using electron microscopy and CNTs have attracted considerable attention in the scientific community since then. CNTs consist of graphitic sheet or sheets wrapped up into cylindrical shape and are allotropes of carbon [7,8]. The length of CNT is measured in up to micrometers and its diameter may reach up to 100 nm depending on the structure. It forms bundles, intertwined in an intricate system. CNT takes either a metallic or semiconducting form, depending on how the

hexagonal rings along the tubular surface are positioned. It is considered for use in a wide range of nanotechnological implementations, such as molecular tanks, polymer matrixes, fillers and more, due to its remarkable properties.

1.2.1. Structure of CNTs

The carbon atoms have a helicity in their arrangement, with a hexagonal pattern in the carbon nanotube structure. The diameter and local symmetry alter the electronic density of states, which creates distinctive electronic properties for the nanotubes [8–10]. There exist two major types of CNTs namely, single-walled (SWCNT) and multi-walled (MWCNT). The diameter of SWCNTs range between 0.7 to 2 nm and they are in the form of rolled up single graphitic sheet. Arc discharge techniques are the most common way of manufacturing SWCNTs. One big disadvantage of this method is that during manufacturing not only CNT but also several by-products are produced. Further separations are required before CNTs are used, and their purity range is approximately 95-98 wt.%. They have both high aspect ratio and high crystallinity.

MWCNTs are usually created by the process of thermal chemical vapor deposition (CVD), which does not need further refining processes. Its diameter spans from 10 to 30 nm, with a 95% purity percentage. SWCNTs and MWCNTs both have an exceptionally high thermal and electrical conductivity, as well as mechanical strength. Additionally, they have a high length to diameter ratio, high crystallinity, and specific surface area. Armchair, zigzag and chiral are the three categories of lattice orientations, differentiated by the angle they are wrapped.

1.2.2. Properties of CNTs

Examining only the cross-sectional area of CNT walls, it is noted that calculated elastic modulus and tensile strength values for individual MWCNTs can be up to 1 TPa and 100 GPa, respectively [11,12]. High quality SWCNTs and arch discharge MWCNTs possess comparatively high tensile strength and modulus values. The tensile strength of CNTs is shown to be more than 10 times higher than any industrial fiber. MWCNTs usually take metallic form and are capable of carrying currents up to 10^9 A cm⁻². Depending on the orientation of the graphene lattice in comparison to the tube axis (chirality), individual CNT walls can take semiconducting or metallic forms. At room temperature, individual

SWCNTs are capable of maintaining a thermal conductivity of $3500 \text{ W m}^{-1} \text{ K}^{-1}$, depending on the area of the wall. This is stronger than a diamond's thermal conductivity.

A few key attributes make CNTs ideal candidates as reinforcement agents in composite materials, including extraordinary strength and stiffness, high resilience, notable thermal and electrical properties and low density. Their stiffness and strength integrated with their remarkably high aspect ratio are additional qualities that make them ideal reinforcing agents.

1.2.3. Applications of CNTs

Because of their extraordinary properties, CNTs have been utilized in diverse nanotechnological applications [9].

There has been an extensive exploration of CNTs on electron field emission materials. At high current density, the emissive electron materials should maintain their stability and accommodate low threshold emission fields. CNTs exactly match these necessary properties for ideal electron emitters, with a high electrical conductivity, chemical stability, nanometer size diameter, and structural integrity. CNT-based emitters, due to the factors listed above, showed definite advantages when compared to conventional emitters [13].

Because of their smooth surface topology, perfect surface specificity, small dimensions and exposure of basal graphite planes in their structures, CNTs stand out in their uses for storage and production of energy as well [14,15].

CNTs are also considered to be the ultimate carbon fiber ever created. The specific strength of carbon-fibers makes intriguing implications for load-bearing reinforcements when used in composites. Therefore, the performance of carbon fiber, an already versatile component of composites, can be enhanced by the addition of CNTs [13,16–21].

1.3. Integration of CNTs into Fiber Reinforced Polymeric Composites (FRPCs)

The integration of CNTs into FRPC by introducing CNTs on the fiber component can be performed by several techniques. Surface properties of fibers such as thermal conductivity and electrical conductivity can be greatly enhanced with the addition of CNTs and the resulting fibers can acquire multifunctionality by the addition of CNTs [22–28]. These techniques can be divided into four main categories based on the medium CNTs are introduced in, namely; CNT growth on fiber, solution-based depositions, sizing of the fibers with CNTs and electrically assisted depositions.

CNTs can be used to coat micron-sized fibers by growing them in situ, using the fiber surface as a substrate for CNT synthesis. This poses numerous advantages, most notably the high control of the growth, uniformity, thickness and density of CNTs, by controlling the process parameters [29,30]. Chemical vapor deposition (CVD), is the most fruitful and pragmatic process of growing CNTs on a substrate. The main disadvantages arise from potential thermal damages to the fibers due to high temperatures required for the CVD, which is expected to weaken their mechanical properties. Downs and Baker recorded some of the first attempts of CVD growth on carbon fibers. Many researchers have studied CVD growth of CNTs on fiber surfaces and achieved remarkable results [31–35].

The “Langmuir-Blodgett (LB)” method includes transferring a CNT monolayer to a substrate during the air/water interface [36,37]. First, the substrate is dipped into the solution, then removed from the solution and this process is repeated to create multilayers of CNTs. It is also known as the “logs-on-a-river” method, and it is a slow, not entirely reliable or reproducible process for manufacturing CNT multilayer films. Its main advantages are its simplicity and cost-effectiveness.

Dip coating is the most elementary form of the Dipping Deposition (DD) method for the deposition of CNTs on the surface of engineering fibers. The fibers are immersed in a dispersion of CNTs. This method is founded on the physiochemical interactions of CNTs and the fiber surface [2]. When immersed in a stable solution containing dispersed CNTs, the fiber and CNTs merge due to capillary, van der Waals and electrostatic forces. The

physiochemical interactions between CNTs and the fiber surface then allows a secure CNT network on the fiber surface by producing the required CNT-to-fiber anchorage.

The most widely-used, large-scale method to deposit CNTs onto surfaces is the Mayer-Rod method [38]. It involves the coating of a substrate with a dispersed CNT solution by using a stainless-steel rod wound by a stainless-steel wire. A heating bar facilitates the post-deposition drying.

The spray coating method diffuses CNTs from a solution on its target by airbrushing the desired amount onto the target. The substrate target is pre-heated to ensure quick drying of the fibers. In order to circumvent any potential agglomeration, CNT dispersion can be sonicated. This method cannot ensure that the CNTs will align in the proper direction. Typically, organic solvents are used for the dispersion of CNTs and this method mainly focuses on the spray coating of prepreg materials [39–43].

Electrophoretic deposition (EPD), used in the processing of ceramics, devices, nanoparticles, supercapacitors, thin films, biomaterials, and more, is a cost-effective and quick wet processing technique. It is effective for use in nanoelectronics, MEMS and flexible electronics [1,7,44,45]. It quickly deposits multilayered CNT films on target substrates from a dispersed CNT solution. Although relatively simple, its main drawbacks are the difficulty in controlling the thickness of the deposited film, as well as the necessity for conducting substrates. It involves two main processes; electrophoresis and deposition. When an electric field is implemented, electrophoresis involves charged particles dispersing in liquid medium moving to a specific electrode. Deposition involves the particles attaching to the electrode surface to create a homogenous deposit. EPD was utilized by many researchers to create hybrid carbon fiber (CF)-CNT surfaces [20,31,46–50].

Self-assembly involves an interaction between the attractive force and interfacial surface tension, occurring between CNTs and the functionalized surface [51]. The surface is functionalized by amino and carboxyl groups or nonpolar groups functionalizing the substrate. The functionalization of the substrate is a driving force for the self-assembly of CNTs. Similar to dip coating, covering a substrate with dispersed CNT solution will form multilayer CNT films. Alternatively, the substrate can be locally charged to guide self-

assembly via coulombic forces. This method can be used in conjunction with dip-pen, nanolithography, photolithography and stamping for patterning.

Inkjet printing of CNT solution is effectively used because of scalability, high deposition rate and high reproducibility. It is used for fine pattern printing rather than large area deposition [52–54].

Spin coating, casting the CNT solution into a substrate and spin-coating to form the CNT films, makes it simpler to produce a monolayer of CNT films [55]. One drawback is the number of repetitions required.

The drop casting method involves dropping the CNT solution to a substrate and air-drying. This produces agglomerated CNTs but is a widely used, non-industrial process.

Although various methods have been reported in the literature to incorporate CNTs and other nanoparticles into FRPCs, there still exists a lack of environmentally friendly, easily scalable methodology for the manufacturing of nano reinforced FRPCs.

This thesis reports the incorporation of SWCNTs into FRPCs, deliberately between polymer-fiber interface, via the spray deposition from their waterborne dispersions onto carbon fabric surfaces prior to the composite fabrication for the first time in the literature as a novel, environmentally friendly and scalable method. Two different spray deposition methods, electrospraying and airbrush spraying were compared while investigating the effects of the content of SWCNTs at the polymer-fiber interface (30 to 90 ppm in the overall composite) on the fracture toughness, flexural properties and interlaminar shear strength of final FRPC structures.

Chapter 2

EXPERIMENTAL

2.1. Materials

SWCNTs (TUBALL BATT) were kindly provided by OCSiAl in the form of waterborne dispersion containing 0.2 wt% SWCNT, 0.4 wt% Polyvinylpyrrolidone (PVP) with SWCNTs having a diameter of 1.8 ± 0.4 nm and a length of more than 5 μm . Further filtration of SWCNT-H₂O dispersion was performed with filter paper MN 640 m Ø 125 mm; Macherey-Nagel, Düren, Germany. 2x2 twill weave carbon fiber fabric woven by Torayca[®] T300-3000 yarn having 245 gsm was provided by KordSA. PTFE tapes were used for initiating cracks for EN 6033 and EN 6034 test. Araldite[®] 2011 adhesive was used for bonding both tensile and mode-I fracture toughness tabs to the specimens. Vacuum bag, peel ply and flow mesh were supplied by Airtech. Biresin resin system was purchased from Sika[®], Germany including; Biresin[®] CR120 resin and Biresin[®] CH 120-6 hardener.

2.2. Preparation of Waterborne SWCNT Dispersions

The commercial SWCNT-H₂O dispersion was diluted to 0.01 wt% SWCNT concentration and further filtered using the vacuum filtration setup shown in Figure 2.1 to remove any agglomerations of SWCNTs. Depending on both the concentration and the amount of SWCNT-H₂O dispersion, multiple filter papers were used as they tended to clog up with every 10-20 ml of SWCNT-H₂O dispersion.



Figure 2.1 Vacuum filtration setup for SWCNT-H₂O dispersions

Dispersions with known concentrations of 0.5, 1.0 and 2.0 ppm SWCNTs were prepared and used for the construction of a calibration curve by UV-Vis Spectroscopy using Shimadzu 3150 UV-VIS Spectrophotometer in the range of 200-500 nm. Concentrations of filtered SWCNT- H₂O dispersions were determined by known dilutions of filtered products by fitting the calibration curve.

2.3. Spray Deposition of SWCNTs

2.3.1. Electro spray Deposition

An in-house built, multiple channel electro spray unit (Figure 2.2) that is capable of spraying 150 cm x 200 cm area with various solvents and adjustable substrate temperature was used for the electro spray deposition of SWCNTs onto CF fabric surfaces.

The in-house built electro spray chamber involved six channeled New Era-1600 Just Infusion[®] pump that is connected to a router for x-y directional movement. The movement of the spraying head was controlled by software using the G code. Depending on the area that will be coated, speed, movement route and step sizes are adjusted by the G code.



Figure 2.2 In-house built electro spray deposition unit

2.3.2. Air Brush Spray Deposition

Airbrush apparatus was purchased from IWATA and connected to the central air pressure line operating at 2 bar. The airbrush spraying process was carried out with a distance of approximately 20 cm between spray nozzle and the CF fabric surface. SWCNT-H₂O dispersion concentration and deposited SWCNT amount per CF fabric surface area were kept analogous to the electro spray deposition with the aim of comparing the two methods. In order to avoid excess water during spraying, the setup shown in Figure 2.3 was used. CF fabrics were then dried in an oven. The time span for the drying process was determined by measuring the weight of drying fabrics in varying time intervals until constant weight was reached. Typically, drying at 50°C for 4 h was the optimum.

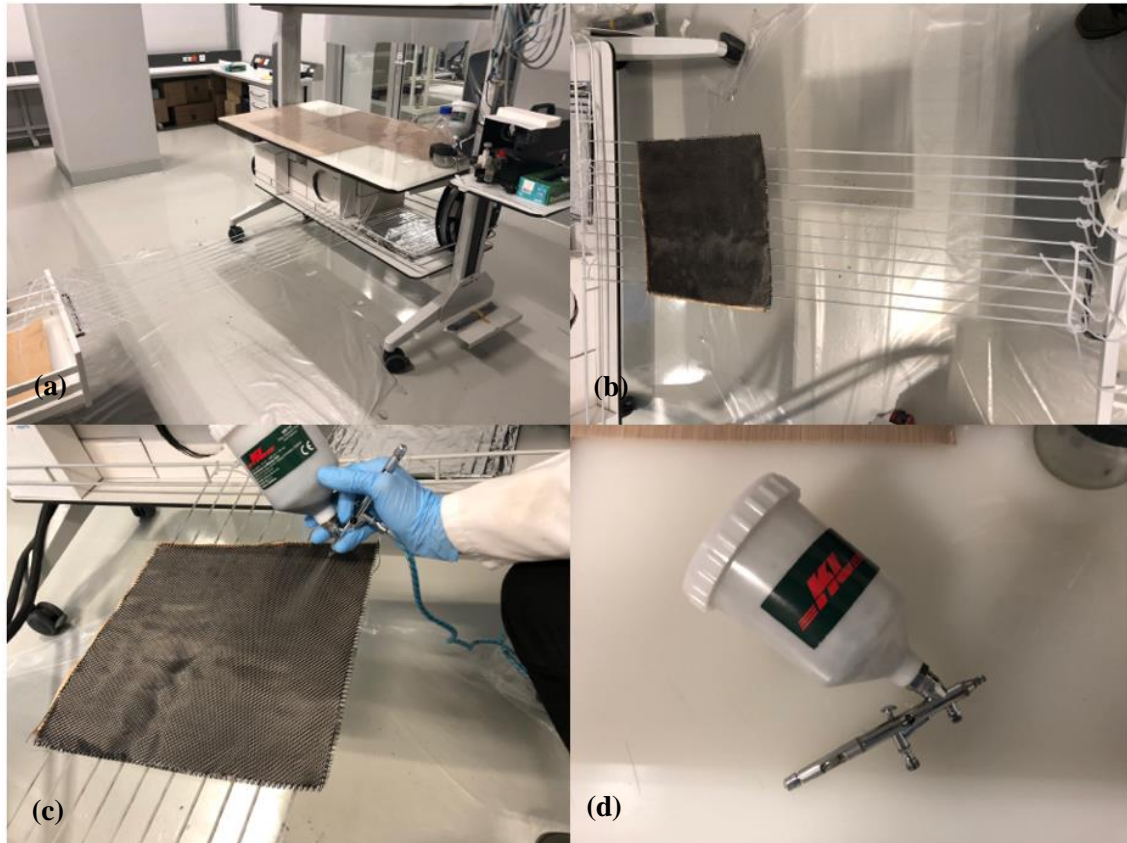


Figure 2.3 (a), (b) and (c) shows airbrush setup, (d) airbrush with extended reservoir

2.4. Manufacturing of SWCNT Incorporated FRPCs

Table 2.1 summarizes all FRPCs manufactured throughout the study including the deposition method, type of CF, the number of CF plies used, surfaces treated, filtration conditions for SWCNT-H₂O dispersion, amount of SWCNTs deposited on each CF fabric surface in mg/m², and total SWCNT concentration in ppm for ten different production trials along with a reference composite material with 0 wt % SWCNTs in each production for comparison purposes.

The naming AB stands for airbrush spray deposition and ES stands for electrospray deposition of SWCNT-H₂O dispersion onto the CF fabric prior to the composite production. The number next to the CNT deposition method (AB or ES) represents the manufacturing order of the FRPC with the mentioned deposition method.

Each composite series/batches were produced using identical carbon fabrics and cured in the same vacuum bagging. The resin system and composition of epoxy and hardener for each composite group was the same; Biresin[®] CR120 resin and Biresin[®] CH 120-6 hardener at a 100:30 weight ratio.

The AB1 and the AB2 are the only batches that were manufactured by using 4 plies of UD fabric. AB1 batch contains samples sprayed using dispersions with two different SWCNTs concentrations (0.01 and 0.1 wt%) and same amount (ml) of SWCNT-H₂O dispersions resulting in overall SWCNT contents of 50 and 500 ppm in the composite panel. In the meantime, AB1 batch also contained a blank control composite plate and another control plate sprayed with the equal amount (ml) of water only to observe possible effects of employing water as the dispersing medium for SWCNTs. SWCNT-H₂O dispersion used for AB1 series was not filtered and SWCNT deposited carbon fabrics of the AB1 batch were kept at room temperature till they were dry.

AB2 batch involves a blank composite sample and two different SWCNT containing samples with the same overall SWCNT contents (50 ppm) in the final composite structure sprayed using dispersions with two different SWCNT concentrations (0.01 and 0.02 wt%) to investigate the effect of SWCNT-H₂O dispersion concentration. In order to investigate the effect of drying conditions, CF fabrics of AB2-0.01 and AB2-0.02 samples were dried at room temperature, while the AB2-0.01-2 sample that is identical to AB2-0.01 was dried at 60°C in an oven.

ES1 batch was manufactured with plain woven CF fabric. In this batch, ES1-0.005 and ES1-0.01 samples were designed to contain 500 ppm of SWCNTs in the final composite, while the ES1-0.02 sample contained 200 ppm of SWCNTs. In addition, SWCNT-H₂O dispersion of ES1-0.01 sample was filtered as described above prior to the spray deposition.

Based on the results obtained from mechanical tests of AB1, AB2 and ES1 batches, essential parameters for the rest of the study such as; concentration of SWCNT-H₂O dispersion, filtration requirement and amount of SWCNT in the overall composite in ppm were determined.

For the rest of the FRPC production trials, 2x2 twill weave CF fabrics were used, the SWCNT-H₂O dispersions contained 0.01 wt % SWCNT concentration and dispersions were filtered before deposition. Aside from that, airbrush spray deposited CFs were dried at 60°C and electro spray deposited CFs came out dry after the process.

Consecutive FRPC plates in batches AB3 and ES2 were manufactured with CF fabrics having dimensions of 400 mm (length) x 400 mm (width). In order to investigate effect of SWCNT deposition method; air brush and electro spray deposited samples for 30, 60 and 90 ppm SWCNT containing FRPC specimens were prepared.

Next, AB4 series having 200 mm x 300 mm dimensions were produced for testing the fracture behavior of FRPCs containing airbrush spray deposited SWCNTs. The SWCNT-H₂O dispersion was deposited only on one sides of the two CF fabric layers forming the mid-plane. Mid-planes of the produced FRCP plates were containing three different concentrations of SWCNT; 6, 12 and 18 mg/m². In the batch AB6, both sides of all the eight CFs were treated with SWCNT for the fracture tests.

The ES4 series were also manufactured to inspect the fracture behavior of FRPC plates containing different amounts of SWCNTs. The number of CF plies was increased from 8 to 12 to investigate its effect on Mode-I and Mode-II fracture toughness of FRPCs.

Lastly, ES/AB series was manufactured in the same vacuum bag to eliminate potential process differences resulting from separate vacuum bags. In addition to previously examined SWCNT concentrations of 30, 60 and 90 ppm, FRPCs were manufactured having as low as 1mg/m² SWCNTs on each CF surface, corresponding to overall SWCNT content of 5 ppm in the final composite. In addition, the effect of pure PVP was investigated in the FRPC structure without SWCNTs, deposited by electro spraying and having identical amounts of PVP as in 30, 60 and 90 ppm SWCNT containing specimens to identify the individual effects of SWCNT and PVP on the mechanical performance of FRPCs.

Table 2.1 List of all manufactured composites

Batch Code	Fabric type	# of plies	Filtration	Composite Code	# of sprayed sides	# of sprayed fabrics	SWCNT per CF surface (mg/m ²)	Overall SWCNT Content in the FRPC (ppm)
AB1	UD fabric	4	no	AB1_REF	0	0	0	0
				AB1-0.01	2	4	11	50
				AB1-0.1	2	4	110	500
				AB1-H ₂ O	0	4	0	0
AB2	UD fabric	4	no	AB2_REF	0	0	0	0
				AB2-0.01	2	4	11	50
				AB2-0.01-2	2	4	11	50
				AB2-0.02	2	4	11	50
ES1	Plain woven	8	-	ES1_REF	0	0	0	0
			no	ES1-0.005	2	8	10	50
			yes	ES1-0.01	2	8	10	50
			no	ES1-0.02	2	8	30	200
AB4	2x2 twill woven	8	yes	AB4_REF	0	0	0	0
				AB4_200	1	2	6	-
				AB4_400	1	2	12	-
				AB4_600	1	2	18	-
AB6	2x2 twill woven	8	yes	AB6_REF	0	0	0	0
				AB6_200	2	8	6	30
				AB6_400	2	8	12	60
				AB6_600	2	8	18	90
ES2	2x2 twill woven	8	yes	ES2_REF	0	0	0	0
				ES2_200	2	8	6	30
				ES2_400	2	8	12	60
				ES2_600	2	8	18	90
ES4	2x2 twill woven	12	yes	ES4_REF	0	0	0	0
				ES4_200	1	2	6	-
				ES4_400	1	2	12	-
				ES4_800	1	2	25	-
				ES4_1600	1	2	50	-

Table 2.2 List of all manufactured composites (continued)

Batch Code	Fabric type	# of plies	Filtration	Composite Code	# of sprayed sides	# of sprayed fabrics	SWCNT per CF surface (mg/m ²)	Overall SWCNT Content in the FRPC (ppm)
ES/AB	2x2 twill woven	8	yes	ES/AB_REF	2	8	0	0
				ES-PVP_200	2	8	0	0
				ES-PVP_400	2	8	0	0
				ES-PVP_600	2	8	0	0
				ES-CNT_30	2	8	1	5
				ES-CNT_200	2	8	6	30
				ES-CNT_400	2	8	12	60
				ES-CNT_600	2	8	18	90
				AB-CNT_30	2	8	1	5
				AB-CNT_200	2	8	6	30
				AB-CNT_400	2	8	12	60
				AB-CNT_600	2	8	18	90

FRPC specimens that were tested for tensile, flexural and shear properties were evaluated and compared based on their overall SWCNT content in the composite structure. However, specimens tested for Mode-I and Mode-II fracture toughness were evaluated based on SWCNT content on each CF surface by mg/m² in the mid-plane.

2.4.1. Vacuum Infusion Process (VIP)

FRPC plates containing SWCNTs were manufactured by the VIP following the electro spray or airbrush spray deposition of SWCNTs onto CF fabrics from SWCNT-H₂O dispersions. Firstly, a heating table was cleaned with XTEND CX-500 Mold Cleaner, then Axel XTEND AMS Semi-Permanent Mold Sealer was applied four times in perpendicular directions in order to cover defects of the heating plate and then Axel XTEND AMS Semi-Permanent Mold Releaser was used, waiting for a minimum of 30 min between each application. Recommended curing temperatures of 120-140°C was used for the resin system on the heating table. All steps of the FRPC manufacturing by VIP are shown in Figures 2.4, 2.5 and 2.6

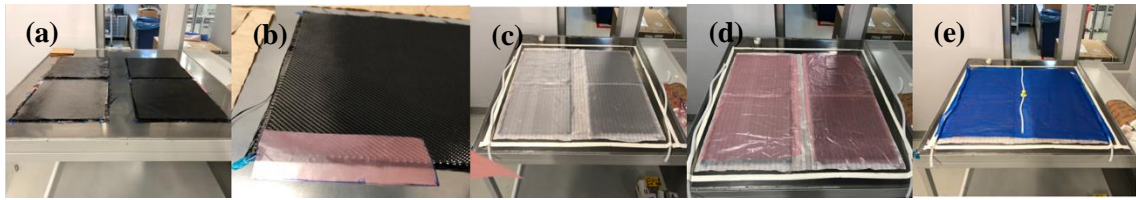


Figure 2.4 VIP steps, (a) alignment of carbon fabrics, (b) PTFE tabs for fracture testing, (c) peel ply, (d) PTFE for easy removal of composites after curing, (e) flow mesh ensuring flow of resin

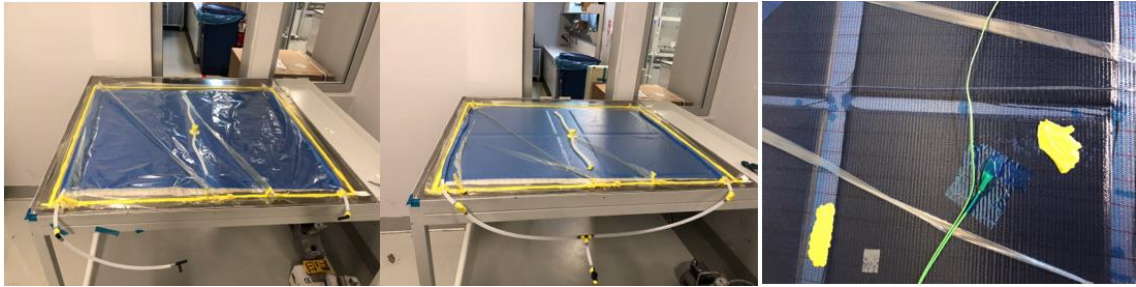


Figure 2.5 Bagging step in VIP

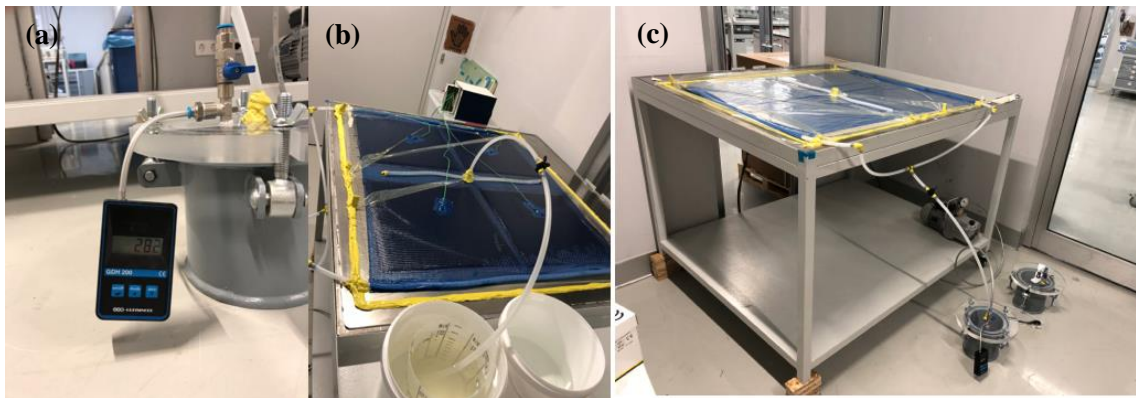


Figure 2.6 VIP steps; (a) vacuum gage, (b-c) resin flow under ambient pressure

Prior to the alignment of the CF fabrics, heat distribution over the heating table was monitored with a thermal camera seen in Fig 2.7(a-b) and placement of the CF fabrics was done accordingly so that each composite plate was subjected to equal temperature. Once the infusion of the resin was completed, vacuum bag was covered with in-house isolator covers seen in Fig 2.7(c) to prevent possible heat loss over the top of the vacuum bag during the curing step.

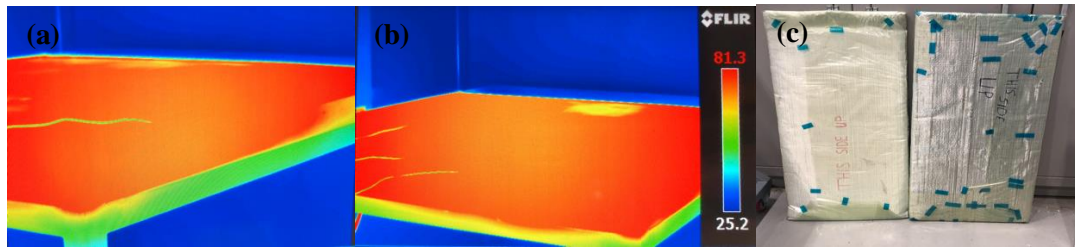


Figure 2.7 (a-b) Thermal imaging of heat table, (c) isolator for VIP

2.4.2. Specimen Preparation

Mechanical test specimens were prepared and cut according to each test standard. For test procedures requiring specimens in small size, ZÜND G3 Digital Ply Cutter was used, while bigger specimens were cut with waterjet.

2.5. Characterization

2.5.1. Thermogravimetric Analysis

Thermogravimetric analyses of chosen samples were performed using Shimadzu DTG-60H Simultaneous DTA-TG instrument to determine the polymer and fiber mass contents of prepared SWCNT containing FRPC samples. Analyses were conducted between 30°C to 800°C with heating rate of 10°C/min under 100 ml/min nitrogen flow. Density of the FRPC specimens measured with density balance and average of three specimens were taken.

2.5.1. Scanning Electron Microscopy (SEM)

Surface morphologies of SWCNT coated carbon fibers were analyzed using Leo SUPRA 35VP FEG-SEM. The images were taken at varying accelerating voltages between 2kV and 10 kV using secondary electron imaging and in-lens imaging modes.

FRPC specimens were also analyzed similarly by SEM after mode-I and mode-II fracture toughness and three-point bending tests. Composites samples were coated with Au-Pd.

2.5.2. Mechanical Testing of FRPC Materials

2.5.2.1. Tensile Test

Tensile properties of FRPCs were tested according to ASTM D 3039 universal test standard [56]. Specimens made of UD CF fabric was cut into dimensions of 250 mm (length) x 15 mm (width) and the specimens made of woven CF fabric was cut into dimensions of 250 mm x 25 mm with varying thicknesses. In order to produce acceptable failure modes, aluminum tabs having dimensions 50 mm x 25 mm with uniform thickness were bonded to both ends of the specimens to protect specimens from surface damage and distribute gripping force equally as shown in Figure 2.8 [3]. Prior to the bonding of the tabs with two component Araldite® 2011 adhesive, smooth surfaces of the FRPC specimens and the aluminum tabs were sanded with 120 grade silicon carbide sandpaper for a better grip of the tab and the specimen. Minimum of 5 specimens were tested for each FRPC sample using INSTRON 5982 100 kN Universal Testing Systems and the data was processed with Bluehill® software. The axial load was applied at a rate of 2 mm/min. Non-contacting video extensometer was used for monitoring the strain and for accurate Poisson's ratio calculations Instron averaging axial and biaxial clip-on extensometer was mounted onto the specimen and connected to the testing machine.



Figure 2.8 Tensile test specimens with aluminum tabs bonded on both ends

2.5.2.2. Mode I Fracture Toughness Test

For Mode-I fracture toughening test, also known as Double cantilever beam (DCB), specimens were cut and prepared according to dimensions seen in Figure 2.9 and all Mode-I specimens were prepared and tested according to ISO EN 6033 test standard [57] as shown in Figure 2.10. The method requires the placement of Polytetrafluoroethylene film (PTFE) of 25 mm x 25 mm x 0.02 mm dimensions for each DCB specimen during the fabrication of composite plates to function as a delamination initiator [58]. Piano hinges were attached to the both sides of the openings by using Araldite® 2011 adhesive. According to the EN 6033 test standard, Mode I interlaminar fracture toughness energy is calculated as follows [57]:

$$G_{IC} = \frac{A}{a \times w} \times 10^6 \quad (2.1)$$

Where G_{IC} is the fracture toughness energy in J/m^2 , a is the propagated crack length in mm, w is the width of the specimen in mm and A is the energy to achieve the total propagated length in J which is the integration of the area of load-cross head displacement graph.

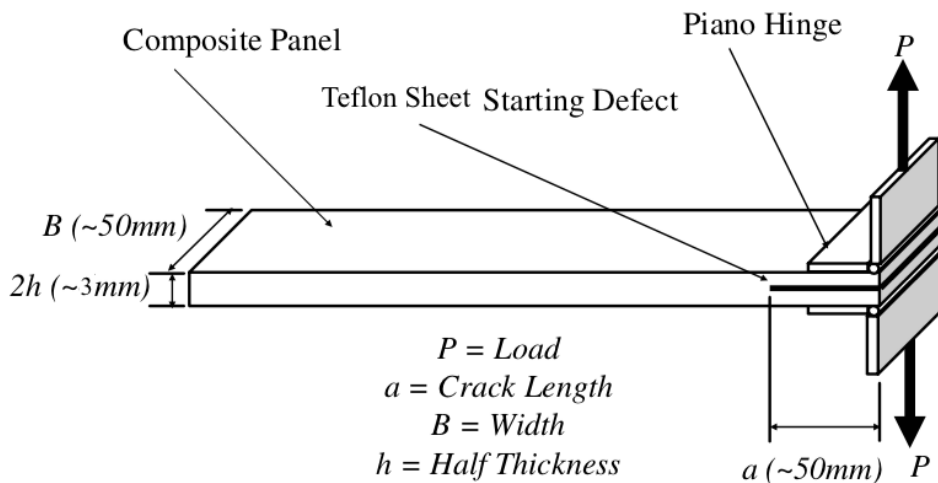


Figure 2.9 Mode I fracture toughness test specimen [59]



Figure 2.10 Mode-I fracture toughness test setup

2.5.2.3. Mode II Fracture Toughness Test

Mode-II fracture toughness test, also known as end-notched flexure (ENF) test was used to measure the interlaminar fracture toughness under in-plane shear deformation mode [58]. ENF test was conducted using INSTRON 5982 100 kN Universal Testing Systems in line with EN 6034 test standard [60]. ENF specimens were prepared according to EN 6034 standard in two ways; specimens were cut from tested EN6033 test specimens having 40mm length with an already initiated crack or new specimens were manufactured with PTFE tabs having dimensions of 40 mm x 25 mm x 0.02 mm for each individual specimen. The specimens' dimensions are given in Figure 2.11. Specimens were positioned under three-point bending fixture and the load was introduced under flexural forces to initiate crack from the tip as seen in Figure 2.12. The specimens were loaded at a displacement rate of 1 mm/min and the detection of crack propagation onset was observed visually. The load and the flexural extension data were recorded during the ENF test. The test was ended after a noticeable crack growth was confirmed by a small load drop. The Mode II fracture toughness energy, G_{IIC} , was measured using the maximum load tolerated by the specimen and the G_{IIC} data was calculated according to Equation 2.2. Calculated G_{IIC} data represents critical strain energy release rate for crack growth for a stated distance.

$$G_{IIC} = \frac{9 \times P \times a^2 \times d \times 1000}{2 \times w(1/4 L^3 + 3a^3)} \quad (2.2)$$

Where G_{IIC} is the mode-II fracture toughness energy, P is the critical load that starts the crack in N, d is the crosshead displacement at crack delamination onset in mm, a is the initial crack length (fixed) in mm, w is the specimen width in mm and L is the span length in mm.

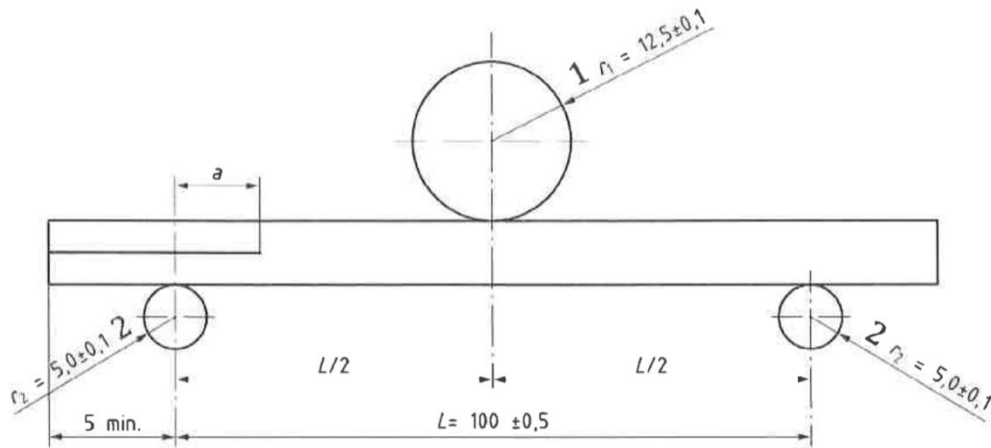


Figure 2.11 Mode II fracture toughness test specimen [60]

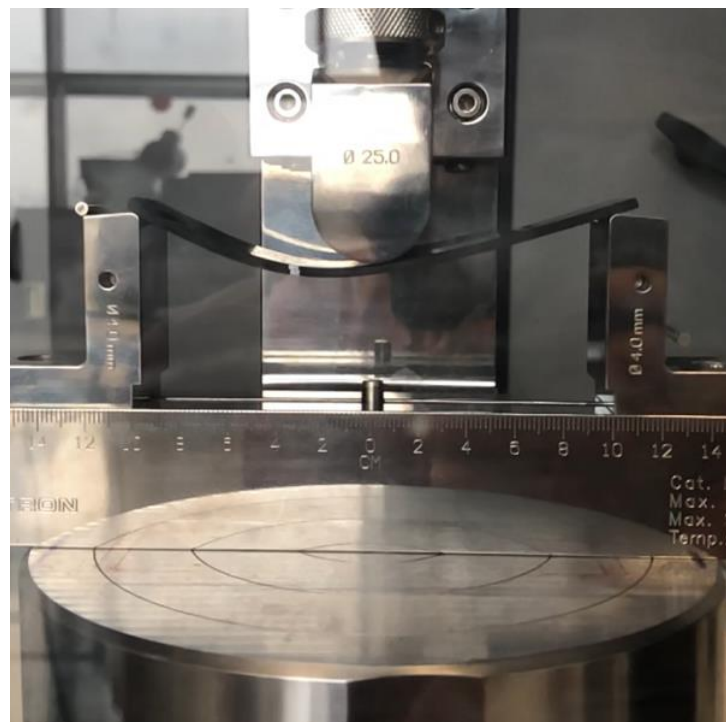


Figure 2.12 Mode-II fracture toughness test setup

2.5.2.4. Three Point Bending Test (Flexural test)

Three-point bending test that involves the bending of the specimen by creating tension in the bottom surface and compression at the top surface [3] was conducted using INSTRON 5982 100 kN in line with ASTM D790 test standard as seen in Figure 2.13 [61].



Figure 2.13 Three-point bending test setup

2.5.2.5. Short Beam Shear Test

The short beam shear test, also known as interlaminar shear test was performed in a three-point bending test setup in order to calculate the interlaminar shear strength (ILSS) of composite samples. The test was conducted using INSTRON 5982 100 kN with a constant cross head rate of 1 mm/min in line with ASTM D2344 test standard [62]. Dimensions of the short beam test specimens are three times the thickness and six times the thickness as width and length, respectively. The ILSS values were calculated using the following equation:

$$F_{sbs} = \frac{0.75 \times P_m}{h \times w} \quad (2.3)$$

where F_{sbs} is the short beam shear strength (ILSS), P_m is the maximum load observed during the test in N, h and w are the thickness and the width of the specimen. The ILSS specimen under flexural load seen in Figure 2.14.



Figure 2.14 Short beam shear test setup

2.5.2.6. V-Notched Shear Test

Shear properties of materials such as shear modulus and shear strength were measured by v-notched shear test in line with ASTM D5379 test standard [63]. Specimens were cut into dimension having 76 mm length and 19 mm width with 90° v-notches on both sides as seen in Figure 2.14. The axial and transverse strain data were measured by Micro Measurements C2A-06- 062LV-350, biaxial shear strain gage. The strain gage was attached to the center of notches with a strong adhesive. The test was conducted using INSTRON 5982 100 kN with a constant cross head rate of 2 mm/min.



Figure 2.15 V-notched test specimens

Chapter 3

RESULTS AND DISCUSSION

3.1. Characterization Results

3.1.1. Characterization of SWCNT Dispersions

The fact that CNTs possess strong Van der Waals interactions among each other is known to cause agglomeration of CNTs into bundles easily, especially in water. The incorporation of SWCNTs onto CF fabrics by both electrospray and airbrush methods requires stable SWCNT aqueous dispersions. The 0.2 wt% SWCNT containing aqueous dispersion in the presence of 0.4 wt% PVP further needed to be diluted with distilled water in order to be practical for spraying. Initially, spraying performances of different concentrations of SWCNT-H₂O dispersions were examined and the effect of filtration of SWCNT-H₂O dispersions analyzed. The filtration of SWCNT-H₂O dispersion was carried out to obtain more stable, agglomeration-free dispersions of SWCNTs; however, the final concentration of the filtered dispersion was unknown. UV-Vis spectroscopy is a reliable method for determining unknown concentrations of CNTs in dispersions. As shown in Figure 3.1, a calibration curve from the UV-Vis spectra of SWCNT-H₂O dispersions with known concentrations (0.5, 1, 2, 5, 10 ppm) was constructed, which was then used to determine concentrations of filtered SWCNT-H₂O dispersions. It was observed that concentrations of SWCNT-H₂O dispersions were approximately halved after the filtration. For example, the absorbance value of SWCNT dispersion with a concentration of 10 ppm after filtration was measured as 0.48 which showed that the actual concentration was 5.8 ppm. The determination of the exact SWCNT concentration after each filtration allowed us to determine the SWCNT content on the CF fabric surface and in the overall composite structure.

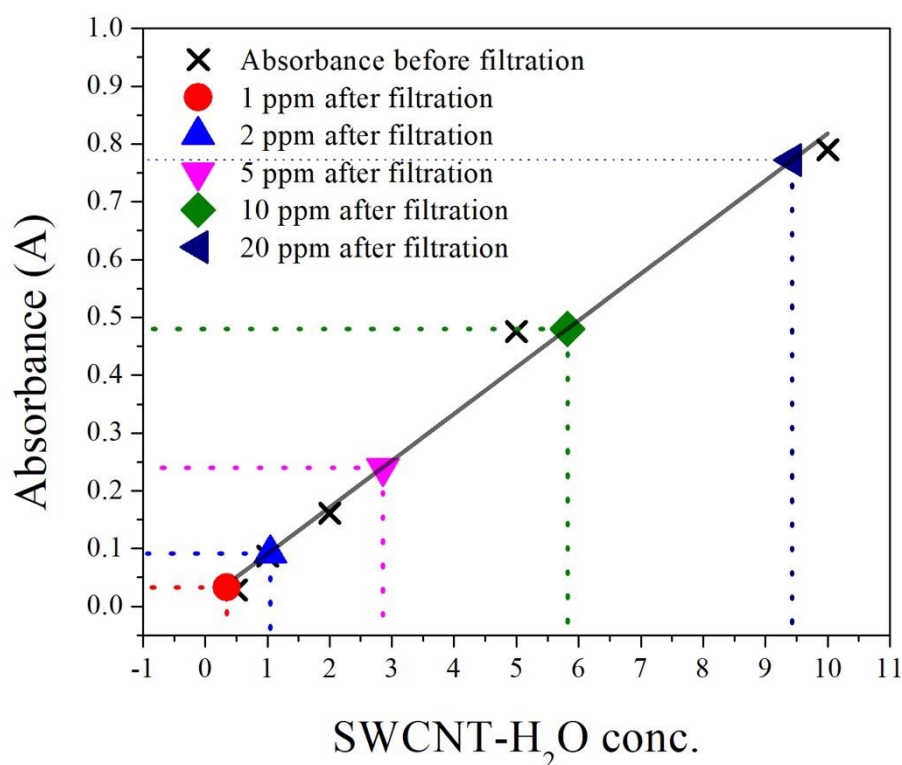


Figure 3.1 Determination of SWCNT concentrations by UV-Vis Spectroscopy after filtration

3.1.2. Spray Deposition of SWCNTs

Electrospray deposition is one of the most versatile tools available for the deposition of nanoparticles by creating nanoscale liquid droplets [64]. Electrospray deposition method allows the deposition of various types of nano materials. For example; Zanjani et al. [65] have employed electrospray deposition of thermally exfoliated graphene oxide sheets on the surface of CF fabric mats and they observed enhancement in mechanical properties of FRPCs fabricated with CFs containing electrospray deposited exfoliated graphene oxide.

Electrospray technique is also used for the generation of thin-film coatings of nanomaterials on various types of substrate. MWCNT thin films on semiconducting and insulating substrates were developed by Maulik et al. [49]. MWCNT particles dispersed in THF-DMF mixture was deposited onto CF surface using electrospray by Li et al. [50] to prepare hybrid CF-CNT structures. They have done an extensive work on analyzing parameters of the electrospray deposition of MWCNTs.

Electrospraying begins when a solution-filled droplet moves through a syringe. It becomes highly electrically charged when it passes through the syringe nozzle due to a DC power supply connection. When the voltage is applied, the particles undergo a Coulomb force that competes with the intrinsic cohesive force inside the particle, reflected in the surface tension. When the Coulomb force exceeds the cohesive force inside the droplets, a Coulombic fission event occurs, which causes atomization. Due to the atomization, the droplet progressively gets smaller and single molecules become ionized. As the particles pass through the nozzle, they maintain their charge and subsequently migrate to a grounded substrate via the electric field [66].

The process and theory behind electrospraying were mainly developed in three stages. In 1882, Lord Rayleigh first explained the theory behind electrospraying as the electrical repulsion on a charged droplet. [4]. He defined a “Rayleigh limit,” the force needed to destabilize the droplet, explained by the equation 1.1, where " σ " is the surface tension, r is the radius of the droplet " ϵ " is the permittivity of the medium:

$$q_r = 8\pi\epsilon^{1/2}\sigma^{1/2}r^{3/2} \quad (1.1)$$

This essentially indicates that the force supplied by the electricity could destabilize the droplets, resulting in a spray pattern that can properly deposit evenly onto the substrate. The dominating force that allows particles to repel each other is coined by the term “Rayleigh discharge” or “Coulomb fission”. In 1914, John Zeleny advanced the understanding of the instability of electrified liquid surfaces [5] and in 1964, Sir Taylor furthered the theory of the atomization of liquid droplets.

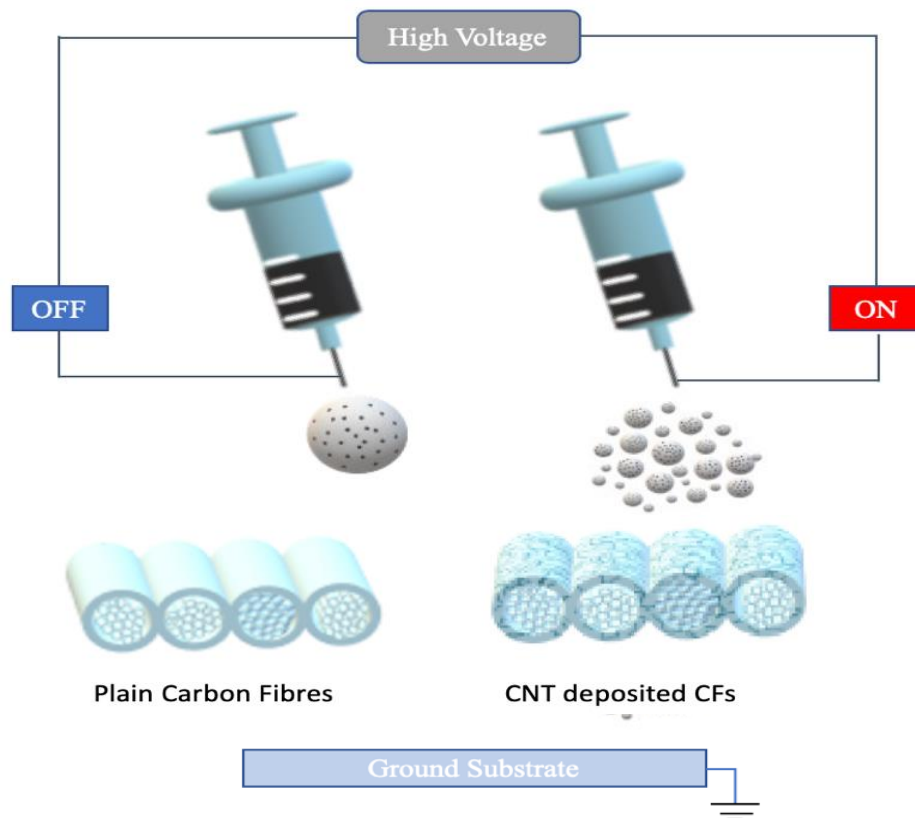


Figure 3.2 Schematic representation of electrospay

During our studies, parameters such as the flow rate, applied voltage, distance from nozzle tip to the grounded surface were needed to be optimized for the in-house built electrospay setup. The electrospay deposition of SWCNTs was achieved by simultaneous spraying from three channels. The high voltage was supplied by attaching crocodiles on metal nozzles. The voltage supply of the three different crocodiles was connected parallel; however, the electric field on each channel was found to be affecting each other. Therefore, the nozzle of each syringe was marked from zero to five for the position of the crocodile on the nozzle (Figure 3.3), and all possible combinations of three syringes at six crocodile positions (6x6x6) were examined for the determination of the ideal spray profile. A total of 216 combinations of crocodile positions were examined and as shown in Figure 3.4, effects of various wiring positions on the electrospay deposition profile was evaluated on white paper substrate.



Figure 3.3 Positioning of crocodiles along syringe nozzles (Ideal positions #2,#4,#3)

An alternative configuration was determined as position #2 for the 1st syringe, position #4 for the 2nd syringe and position #3 for the 3rd syringe for the crocodile on metal nozzles as shown in Figure 3.4. It should be noted that, the determination of a neat spray profile and having a narrow particle size distribution with optimized parameters was critical to achieve homogenous SWCNT deposition.

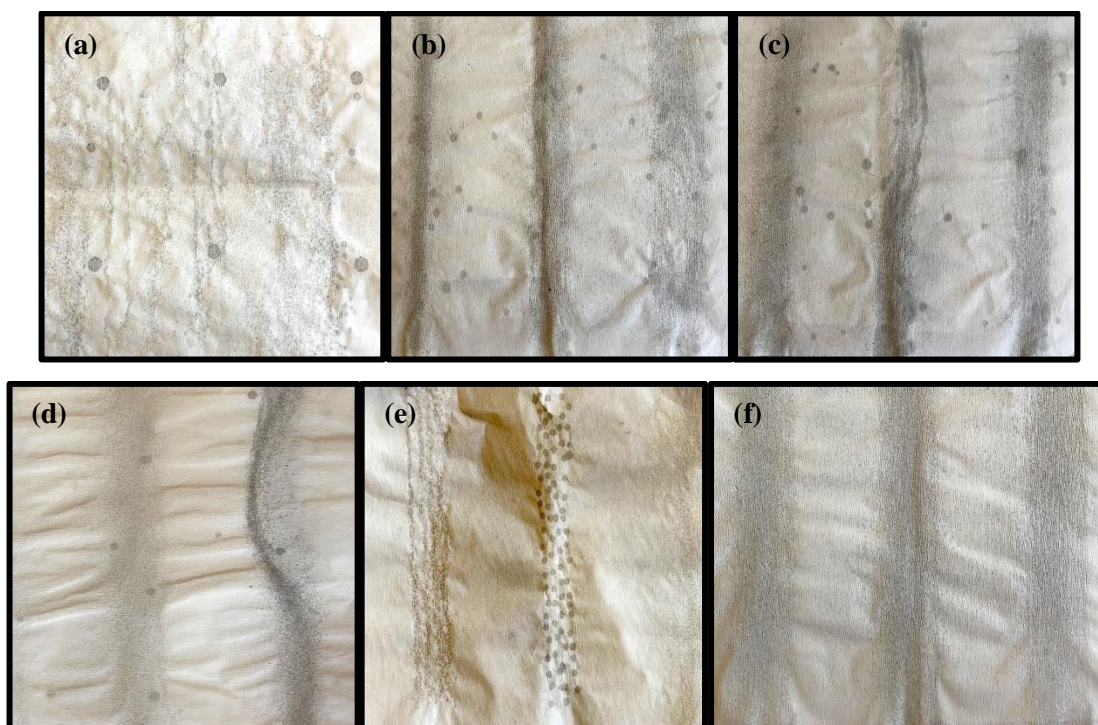


Figure 3.4 Effects of different crocodile positions along nozzles on the spraying profile (on white paper) (a) #1#1#1 (b) #1#2#4 (c) #2#5#2 (d) #1#4#4 (e) #1#0#3 (f) #2#4#3

Alternatively, airbrush spraying technique that uses air pressure to atomize particles in a liquid droplet was utilized to deposit SWCNTs onto CF fabric from aqueous dispersions. Airbrush spraying is generally used for spraying micro particles and painting surfaces. Even though airbrush spraying method is more practical with simpler parameters, this technique has a few disadvantages in terms of spraying onto dry CF fabric. Unlike electrospray deposition, significant amount of water remained on CF fabrics after airbrush spraying. In order to dry airbrush sprayed CF fabrics prior to FRPC manufacturing, they were either kept in a clean environment at room temperature for several days or placed into an oven at 50-60°C till they dry. CF fabrics were susceptible to contamination or to be damaged by both drying methods. Secondly, the homogeneity of nanoparticles while spraying was highly user dependent, not controlled with an automated setup like the electrospray deposition. Table 3.1 summarizes the comparison of the two spray deposition processes.

Table 3.1 Comparison of airbrush and electrospray methods

Airbrush	Electrospray
Fabrics need to be dried after the process	Fabrics are dry after the process
Only needs 2 bar pressure	Requires high voltage
Faster deposition rate 400ml/h	Deposition rate between 120ml/h (max) and 40ml/h (min)
Preform formation (CF fabrics became stiffer)	No preform formation of stiffening of CF fabrics
Homogeneity is user dependent	Homogenous deposition
Easily adaptable to large scale production	High capital investment for the integrated into large scale production

Eight different batches of FRPC systems were manufactured throughout this study. Each composite system was initially designed to have comparable sample among its own group; however, manufacturing conditions of all batches were aimed to be analogous to each other so that specimens of different batches were comparable as well.

3.1.3. SEM Analysis of Sprayed CF Fabrics

SEM is one of the essential characterization techniques that has enabled the optimization of both electrospray and airbrush spray deposition parameters by the investigation of the surface morphology of SWCNT deposited CF fabrics. The effect of varying the electrospray deposition voltage, flow rate of the SWCNT-H₂O dispersion, scan rate of the spraying head and SWCNT-H₂O concentration were investigated through SEM micrographs. In the light of these analysis, parameters of electrospray deposition and airbrush spraying have been optimized.

Prior to the composite production, in order to analyze the homogeneity of SWCNT distribution on the CF fabric, airbrush and electrospray coated CF fabrics were examined and compared at optimum SWCNT amounts per CF fabric area as shown in SEM images in Figures 3.5 to 3.13. In general, a homogeneous distribution of SWCNTs were observed by both spraying methods with low amount of SWCNTs under optimized conditions; however, the presence of the PVP film was more profound with increasing SWCNT deposition amount.

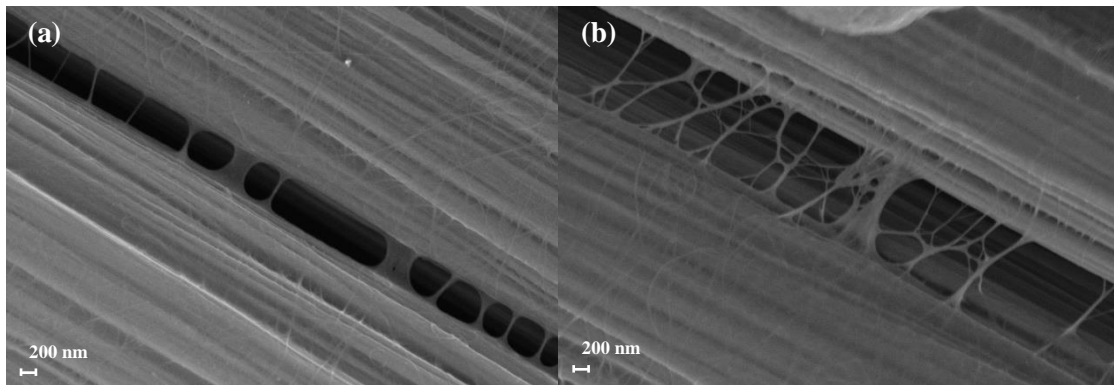


Figure 3.5 SEM images of airbrush sprayed 6 mg/m² SWCNT on CF fabric; (a-b) 40Kx at 3kV

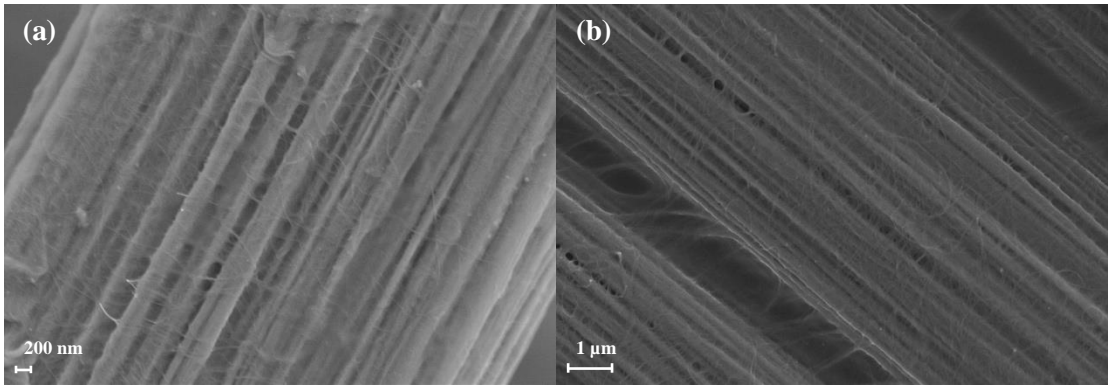


Figure 3.6 SEM images of 6 mg/m² SWCNT electrospayed on CF fabric at 13.5kV; (a) 40Kx at 3kV (b) 25Kx 3kV

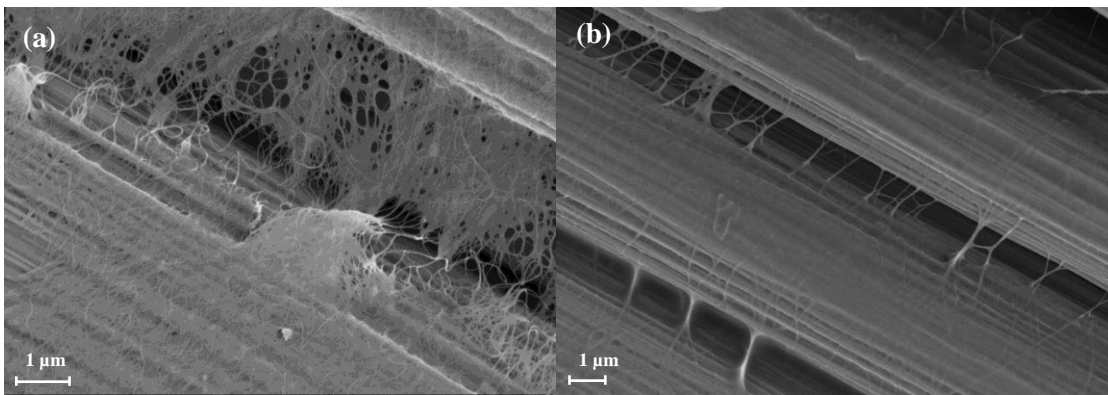


Figure 3.7 SEM images of airbrush sprayed 12 mg/m² SWCNT on CF fabric (a) 30Kx at 3kV (b) 20Kx at 3kV

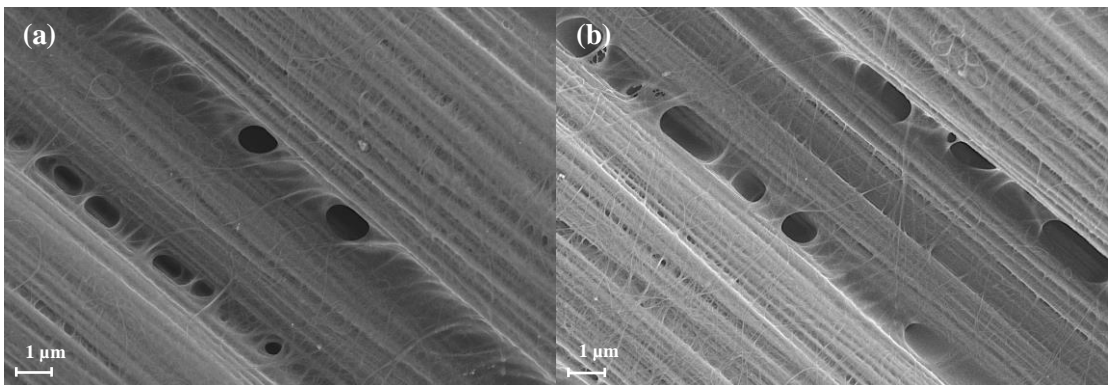


Figure 3.8 SEM images of 12 mg/m² SWCNT electrospayed on CF fabric at 13.5kV; (a-b) 20Kx at 3kV

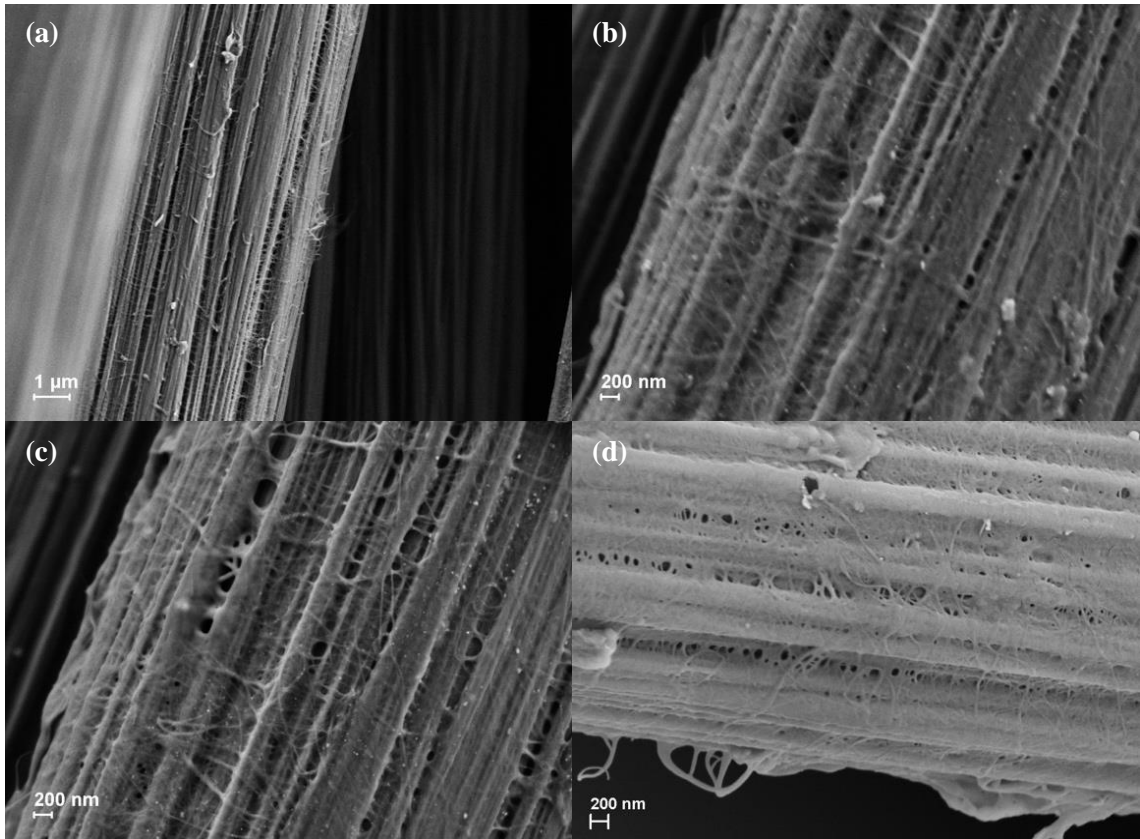


Figure 3.9 SEM images of 18 mg/m² SWCNT electrospayed on CF fabric at 13.5kV (a) 20Kx at 2kV (b-c) 50Kx at 2kV (d) 50Kx at 5kV

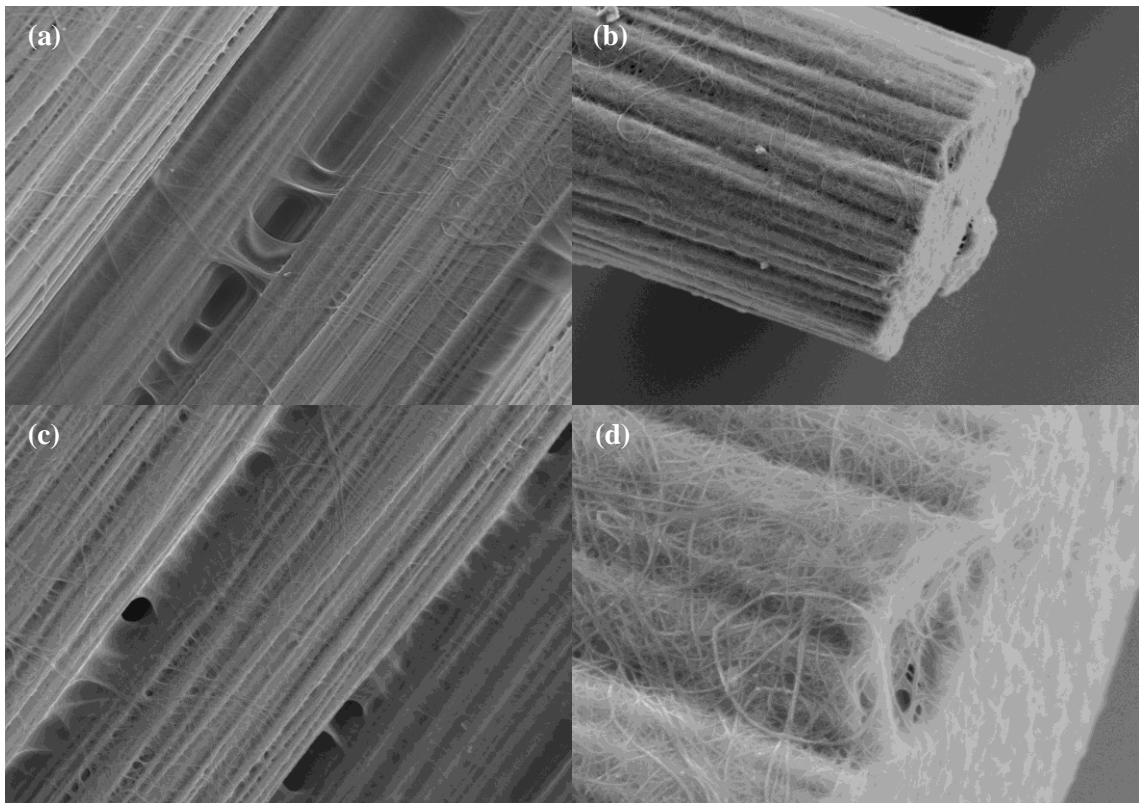


Figure 3.10 SEM images of airbrush sprayed 18 mg/m² SWCNT on CF fabric (a,c) 20Kx at 3kV (b) 20Kx at 3kV (d) 100Kx at 3kV

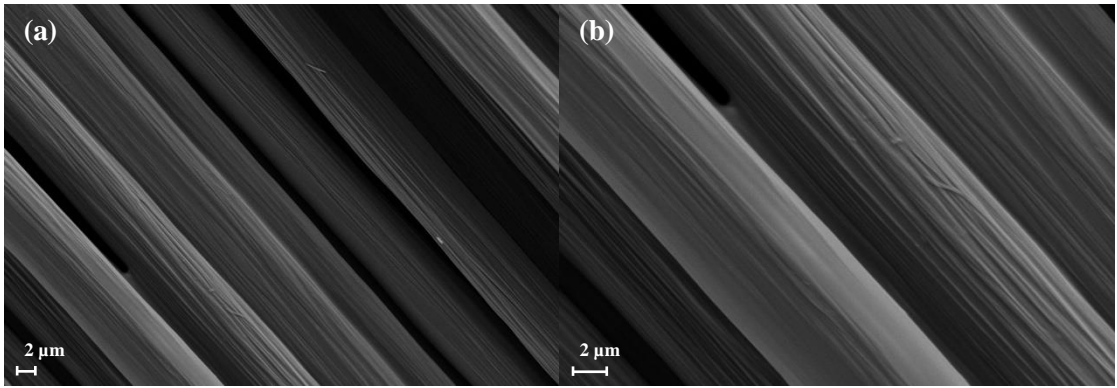


Figure 3.11 SEM images of PVP only electrospayed on CF fabric equivalent to 6 mg/m² SWCNT deposition conditions at 13.5kV, (a) 5Kx at 3kV (b) 10Kx at 3kV

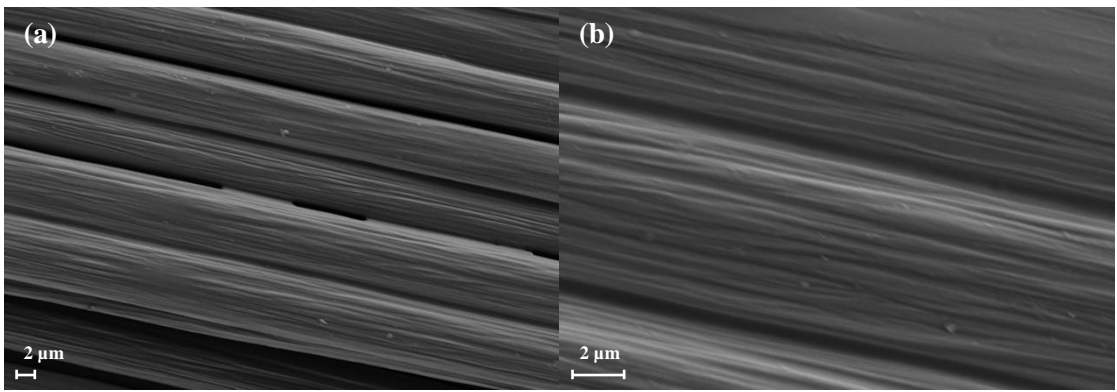


Figure 3.12 SEM images of PVP only electrospayed on CF fabric equivalent to 12 mg/m² SWCNT deposition conditions at 13.5kV (a) 5Kx at 3kV (b) 15Kx at 3kV

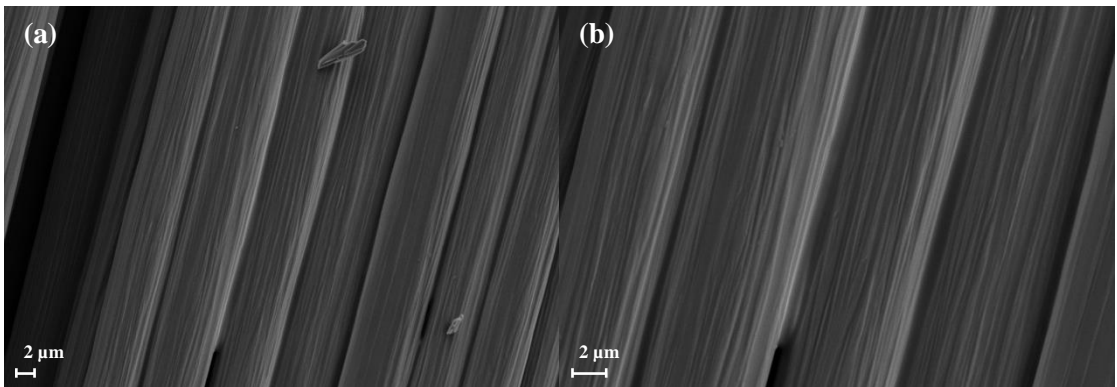


Figure 3.13 SEM images of PVP only electrospayed CF fabric equivalent to 18 mg/m² SWCNT deposition conditions at 13.5kV (a) 5Kx at 3kV (b) 10Kx at 3kV

3.2. Structural Characterization of FRPC Panels

In order to determine the average density, fiber/resin ratio by wt% and void content of SWCNT containing FRPC plates manufactured by VIP, a series of characterizations were carried out. TGA measurements were conducted for the decomposition of the resin component of FRPCs to determine the fiber and resin ratio of the samples. With the help of knowing fiber-resin content and density of each plate, we were able to determine the void content of each composite structure as summarized in Table 3.2.

Table 3.2 Properties of manufactured composites, average density, void content, fiber-resin ratio

Batch Code	Composite Code	Ave. Density	Void Content	Fiber wt%	Resin wt%
		g/cm ³	volume %		
AB1	AB1_REF	1.554	0.038	75.71	24.29
	AB1-0.01	1.546	1.451	71.51	28.49
	AB1-0.1	1.534	0.447	71.97	28.03
	AB1-H ₂ O	1.551	0.238	75.72	24.28
AB2	AB2_REF	1.408	0.077	54.21	45.79
	AB2-0.01	1.417	0.370	56.34	43.66
	AB2-0.01-2	1.414	0.670	56.54	43.46
	AB2-0.02	1.401	1.686	56.78	43.22
ES1	ES1_REF	1.423	1.936	60.86	39.14
	ES1-0.005	1.419	1.146	58.43	41.57
	ES1-0.01	1.431	1.687	61.54	38.46
	ES1-0.02	1.412	1.962	59.18	40.82
AB4	AB4_REF	1.456	1.776	65.56	34.44
	AB4_200	1.444	2.880	66.22	33.78
	AB4_400	1.444	2.480	65.32	34.68
	AB4_600	1.451	1.897	65.08	34.92
AB6	AB6_REF	1.455	1.652	65.13	34.87
	AB6_200	1.461	1.088	64.78	35.22
	AB6_400	1.458	1.557	65.37	34.63
	AB6_600	1.453	0.956	63.28	36.72

Table 3.2 Properties of manufactured composites, average density, void content, fiber-resin ratio (continued)

Batch Code	Composite Code	Ave. Density	Void Content	Fiber wt%	Resin wt%
		g/cm ³	volume %		
ES2	ES2_REF	1.461	1.398	65.41	34.59
	ES2_200	1.450	1.281	63.55	36.45
	ES2_400	1.458	0.877	63.86	36.14
	ES2_600	1.454	0.719	62.90	37.10
ES4	ES4_REF	1.453	2.247	66.15	33.85
	ES4_200	1.451	1.875	65.03	34.97
	ES4_400	1.457	1.055	64.10	35.90
	ES4_800	1.459	0.839	63.93	36.07
	ES4_1600	1.456	0.402	62.50	37.50
ES/AB	ES/AB_REF	1.448	0.389	61.14	38.86
	ES-PVP_200	1.443	0.719	60.15	39.85
	ES-PVP_400	1.441	0.692	60.80	39.20
	ES-PVP_600	1.442	0.865	61.29	38.71
	ES-CNT_30	1.435	0.405	59.19	40.81
	ES-CNT_200	1.423	1.136	58.90	41.10
	ES-CNT_400	1.426	0.964	59.12	40.88
	ES-CNT_600	1.423	1.444	59.68	40.32
	AB-CNT_30	1.433	0.830	59.78	40.22
	AB-CNT_200	1.436	1.267	61.24	38.76
	AB-CNT_400	1.430	0.846	59.42	40.58
	AB-CNT_600	1.430	0.066	57.70	42.30

Specimens with the highest SWCNT content in each batch exhibited higher percentage of resin in their structure. This in fact indicates that as the SWCNT amount increased, resin absorption also increased showing that additional anchoring points were introduced for the resin with increasing SWCNT amount on the CFs fabric surface.

3.3. Mechanical Characterization of FRPCs

For the manufactured SWCNT containing and control FRPC panels, detailed mechanical tests, namely; ASTM D3039 tensile test, EN6033 Mode-I and EN6034 Mode-II, ASTM D790 three-point bending test, ASTM D2344 short beam shear strength test and ASTM D5379 shear test were carried out.

3.3.1. Tensile Tests

Tensile testing of selected samples allowed us to understand the effect of interfacially located SWCNTs on the essential mechanical properties of FRPC materials such as; ultimate tensile strength, strain at failure, tensile chord modulus of elasticity and Poisson's ratio. The analyses were primarily made for composite batches that were manufactured within the same vacuum bag. Table 3.3 summarizes the elastic modulus, tensile strength and tensile strain at break values for airbrush sprayed FRPC samples.

Table 3.3 Tensile test results of airbrush sprayed AB1 batch

Sample	Tensile Modulus	Tensile Strength	Tensile Strain
	(GPa)	(MPa)	(%)
AB1_REF	63.9 ± 1.6	1283.0 ± 66.60	1.85 ± 0.08
AB1-0.01	67.3 ± 0.2	1388.8 ± 26.00	2.02 ± 0.03
AB1-0.1	64.7 ± 0.4	1399.9 ± 9.90	2.05 ± 0.01
AB1-H ₂ O	64. ± 0.76	1342.2 ± 39.80	1.92 ± 0.04

AB1_H₂O sample, which was produced by spraying the same amount of only water as the SWCNT sprayed samples AB1-0.01 and AB1-0.1, showed very small deviations in its tensile properties from the control sample, showing that water spraying has no significant effect. In general, tensile properties of airbrush SWCNT sprayed FRPC samples slightly increased with respect to the control samples. The introduction of 50 ppm of SWCNT onto CF fabric with airbrush spraying from a 0.01 wt% SWCNT containing aqueous dispersion (AB1-0.01) increased the tensile modulus by 4% and the tensile strength by 7%, whereas the tensile strain increased by 9%. With the introduction of 500 ppm of SWCNTs from a 0.1 wt% SWCNT containing aqueous dispersion (AB-0.1), the tensile strength increased by 8% and tensile strain increased by 10.4%. It should

be noted that the processing of 0.1 wt % SWCNT-H₂O dispersion was difficult for airbrush spraying and not suitable for electrospraying.

In the case of AB2 series, which had the same type and number of plies as AB1, there exists a huge difference in elastic modulus, tensile strength and tensile strain values compared to AB1 series as shown in Figure 3.14 and Table 3.4, which can be explained by the increased resin content of each composite plate in AB2 series as given in Table 3.2. The higher fiber volume in AB1 series explains why UD fabric dominated AB1 has significantly higher values than AB2.

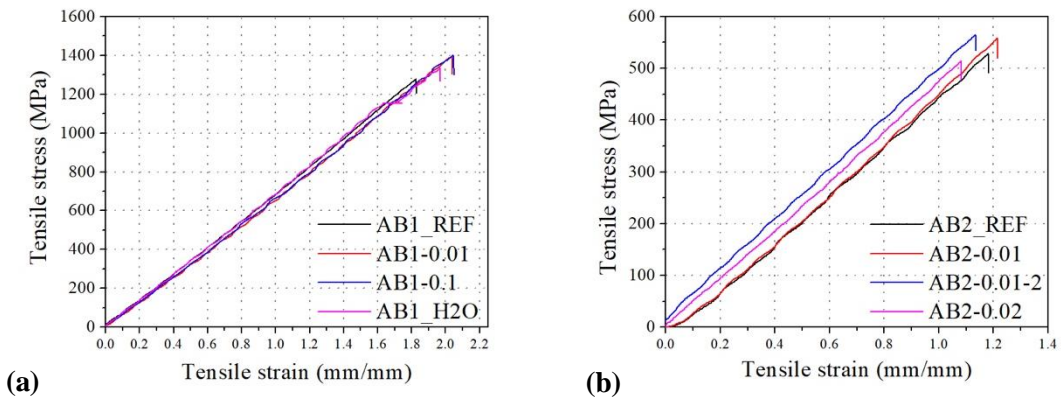


Figure 3.14 Tensile stress versus strain curves of (a) AB1, (b) AB2 batches

Table 3.4 Tensile test results of airbrush sprayed AB2 batch

Sample	Tensile Modulus	Tensile Strength	Tensile Strain
	(GPa)	(MPa)	(%)
AB2_REF	43.04 ± 0.81	527.97 ± 8.58	1.14 ± 0.03
AB2-0.01	46.14 ± 1.34	564.62 ± 19.36	1.23 ± 0.04
AB2-0.01-2	48.26 ± 1.1	565.49 ± 0.45	1.23 ± 0.06
AB2-0.02	45.52 ± 0.50	519.65 ± 7.71	1.13 ± 0.04

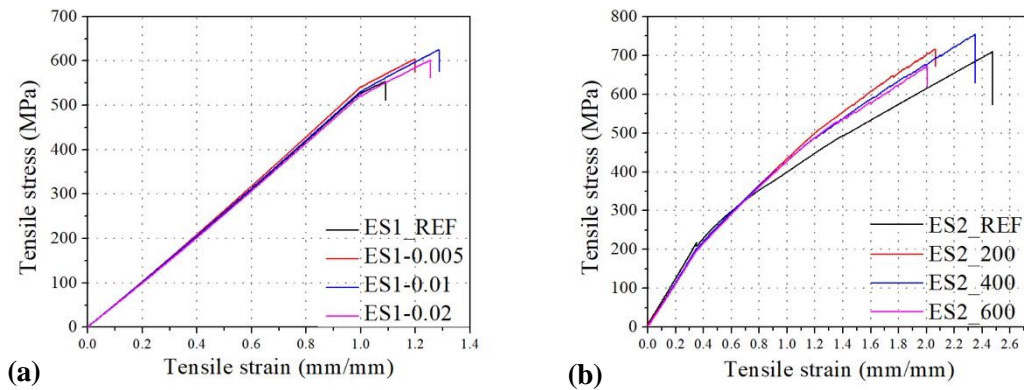
A similar trend was observed for electrospray deposited samples, with a slight increase in tensile properties for most of the samples as summarized in Table 3.5 and Table 3.6.

Table 3.5 Tensile test results of electrospayed ES1 batch

Sample	Tensile Modulus	Tensile Strength	Tensile Strain	Poisson's ratio
	(GPa)	(MPa)	(%)	(%)
ES1_REF	51.36 ± 0.94	547.17 ± 66.66	1.08 ± 0.15	0.059 ± 0.007
ES1-0.005	52.30 ± 00	604.48 ± 00	1.20 ± 00	0.052 ± 00
ES1-0.01	51.63 ± 0.38	620.99 ± 17.51	1.28 ± 0.05	0.062 ± 0.002
ES1-0.02	51.05 ± 1.03	590.54 ± 15.77	1.24 ± 0.04	0.068 ± 0.002

ES1 was the first batch that is tested for tensile properties. It should be noted that, the incorporation of 50 ppm of SWCNT to the FRPC sample with plain woven fabric from a 0.01wt% SWCNT dispersion resulted in the highest improvement in the tensile strength as shown in Table 3.5.

Figure 3.15 Tensile stress versus strain curves of (a) ES1, (b) ES2 batches



In the case of ES2 series, the tensile strength of FRPCs improved by 9.1% upon the incorporation of 60 ppm SWCNTs into the overall composite structure in ES2_400 sample. With the incorporation of 90 ppm SWCNTs, tensile properties reduced as seen in Table 3.6. On the other hand, the tensile modulus of ES2 series showed slight decrease or no change.

Table 3.6 Tensile test results of electrospayed ES2 batch

Sample	Tensile Modulus	Tensile Strength	Tensile Strain	Poisson's ratio
	(GPa)	(MPa)	(%)	(%)
ES2_REF	59.50 ± 0.58	692.97 ± 49.54	2.204 ± 0.247	0.02 ± 0.004
ES2_200	56.48 ± 0.16	701.32 ± 33.06	1.988 ± 0.068	0.04 ± 0.010
ES2_400	58.38 ± 0.29	756.10 ± 12.11	2.233 ± 0.120	0.02 ± 0
ES2_600	57.29 ± 0.10	669.82 ± 10.05	1.967 ± 0.127	0.027 ± 0.006

Table 3.7 Tensile test results of airbrush sprayed or electrospayed ES/AB batch

Sample	Modulus (Chord)	Tensile Strength	Tensile Strain
	(GPa)	(MPa)	(%)
ES/AB_REF	59.56 ± 0.53	664.2 ± 26.95	1.67 ± 0.16
ES-PVP_200	54.19 ± 1.41	677.6 ± 32.79	1.78 ± 0.16
ES-PVP_400	61.47 ± 2.03	680.6 ± 27.35	1.9 ± 0.12
ES-PVP_600	54.32 ± 0.80	659.3 ± 25.80	2.1 ± 0.26
ES-CNT_30	54.6 ± 1.14	675.3 ± 26.5	2.08 ± 0.17
ES-CNT_200	56.72 ± 0.96	710.4 ± 23.2	2.24 ± 0.10
ES-CNT_400	59.92 ± 0.22	724.7 ± 20.1	1.78 ± 0.08
ES-CNT_600	54.02 ± 1.11	652.3 ± 30.5	2.05 ± 0.08
AB-CNT_30	53.17 ± 0.59	671.5 ± 25.3	1.98 ± 0.07
AB-CNT_200	57.54 ± 1.13	700.4 ± 17.6	2.16 ± 0.11
AB-CNT_400	56.1 ± 1.05	708.2 ± 16.6	1.87 ± 0.08
AB-CNT_600	51.38 ± 1.74	647.5 ± 19.5	2.09 ± 0.12

The ES/AB series was the only batch that involved the fabrication of separate composite panels from both airbrush and electrospayed CF fabrics in the same vacuum bag. As seen in the Table 3.7, the incorporation of only PVP by electrospaying equivalent amounts to 30, 60 and 90 ppm SWCNT deposited samples has resulted in up to 2% increase in tensile strength (ES-PVP_200, _400 and _600); however, the incorporation of 60 ppm of SWCNTs increased tensile strength of the final composite by 9.1% when electrospayed (ES-CNT_400) and 6.6 % when airbrush sprayed (AB-CNT_400) in comparison to reference sample (ES/AB_REF). By both spraying methods (AB & ES), the composite

samples having the highest concentration, 90 ppm of SWCNTs, have shown a significant drop in their tensile modulus and tensile strength values. Composite samples having 30 ppm SWCNTs in their structure has shown 6.9% and 5.5% improvement in tensile strength values for ES-CNT_200 and AB-CNT_200, respectively, still lower than that of 60 ppm SWCNT incorporated samples. Finally, composite samples containing 5 ppm SWCNTs have shown little or no improvement in tensile values, implying that the incorporation of as low as 5 ppm SWCNTs had no effect.

3.3.2. Mode I Fracture Toughness Test Results

Mode-I fracture toughness test is a critical method that evaluates materials' resistance to the force normal to fracture surface, which is also known as double cantilever beam test. For the ES1 batch, composite samples with 50 ppm SWCNTs showed decreased fracture toughness compared to the control sample, which later on increased by up to 13% with increasing SWCNT content (200 ppm) as summarized in Table 3.8 and shown in Figure 3.16 (a). It should be noted that ES1 series was manufactured with plain woven CF fabric and these composite sample were not comparable with other series. In addition, although G_{IC} improvement was observed only for ES1-0.02 sample that was fabricated from CF fabrics containing 30 mg/m² SWCNTs on each surface, lower amount of SWCNTs were introduced onto CF fabric surfaces in the following batches due to processing difficulties at high SWCNT amounts per CF fabric surface area.

Table 3.8 Mode-I fracture toughness test results of ES1 batch

Sample	Corrected G_{IC}	Change
	(N/m)	(%)
ES1_REF	539 ± 20	-
ES1-0.005	501 ± 19	-7.0
ES1-0.01	481 ± 8	-10.8
ES1-0.02	608 ± 44	12.8

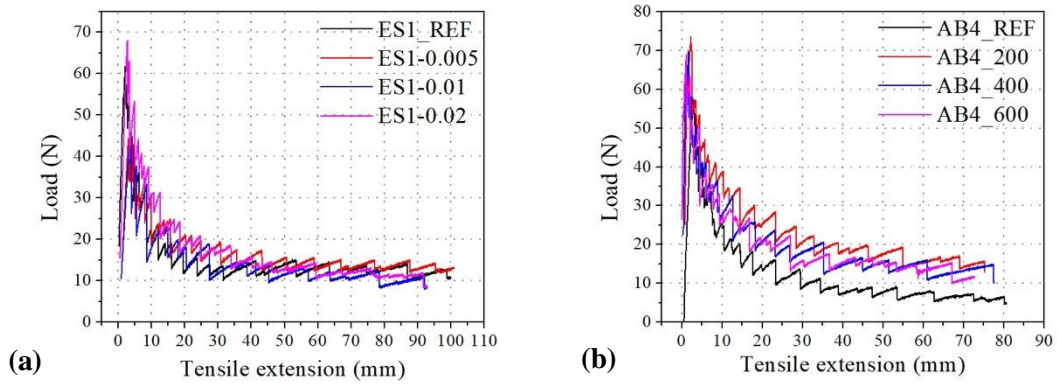


Figure 3.16 Load versus tensile extension graph, Mode-I fracture toughness test of (a) ES1, (b) AB4 batches

Composite samples of AB4 batch with twill CF fabric has shown a significant increase in G_{IC} values compared to reference specimen produced together with SWCNT containing composite samples. Improvements in the G_{IC} values by 42%, 29% and 18% were observed with respect to the reference, for 6, 12 and 18 mg/m^2 SWCNT containing composites, which correspond to 30, 60 and 90 ppm SWCNT containing composite samples, respectively. However, it should be noted that AB4_REF sample showed a very high deviation from its mean G_{IC} value. Opposite to the electrospayed samples in Table 3.8, Mode-I fracture toughness values showed the highest increase with the lowest SWCNT addition in the airbrush sprayed samples and the improvement with respect to the reference decreased as SWCNT amount was increased. The G_{IC} values obtained from FRPCs involving of airbrush sprayed CF fabrics showed decreasing tendency as the SWCNT content on the CF fabric surface increased.

Table 3.9 Mode-I fracture toughness test results of AB4 batch

Sample	Corrected G_{IC}	Change
	(N/m)	(%)
AB4_REF	389 ± 101	-
AB4_200	504 ± 12	42.3
AB4_400	456 ± 54	28.8
AB4_600	419 ± 23	18.3

In the case of ES2 batch with 2x2 twill woven CF fabric, independent from the SWCNT content, all samples showed similar improvements around 13% in the G_{IC} values with

respect to the control sample produced in the same batch as summarized in Table 3.10 and shown in Figure 3.17-(a).

Table 3.10 Mode-I fracture toughness test results of ES2 batch

Sample	Corrected G_{IC}	Change
	(N/m)	(%)
ES2_REF	438 ± 23	0
ES2_200	498 ± 15	13.8
ES2_400	495 ± 13	13.0
ES2_600	493 ± 25	12.5

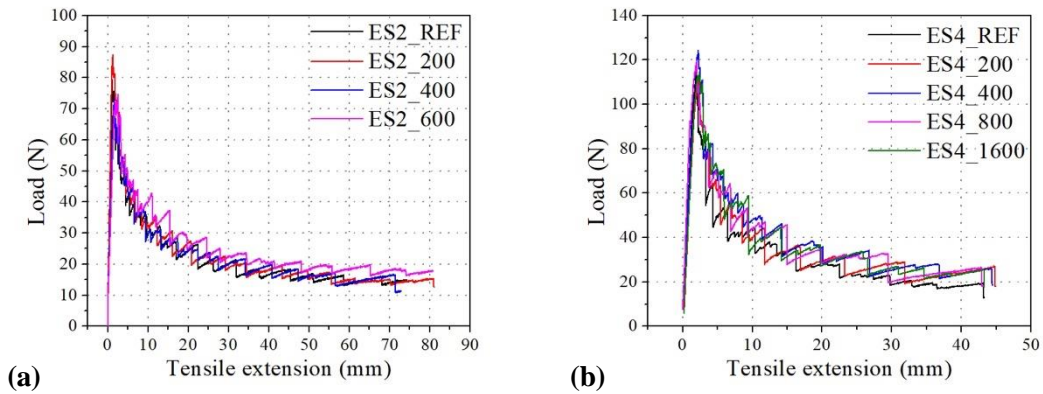


Figure 3.17 Load versus tensile extension graph, Mode-I fracture toughness test of (a) ES2, (b) ES4 batches

In order to investigate the effect of the number of plies, ES4 batch was produced with 12 plies in comparison with eight plies in ES2 series. Interestingly, improvements up to 20% was observed in G_{IC} values with respect to the reference composite material when the number of plies was increased as summarized in Table 3.11 and shown in Figure 3.17-(b). ES4_400 sample that showed up to 20% improvement in an 12 ply composite structure had identical SWCNT amount to the ES2_400, which showed 13% improvement in the G_{IC} value in an 8 ply composite structure.

Table 3.11 Mode-I Fracture Toughness Test Results of ES4 Batch

Sample	Corrected G_{IC}	Change
	(N/m)	(%)
ES4_REF	434 ± 43	0
ES4_200	461 ± 20	6.4
ES4_400	525 ± 8	21.0
ES4_800	494 ± 26	14.1
ES4_1600	499 ± 5	15.2

3.3.3. Mode II Fracture Toughness Test Results

Mode-II fracture toughness test was conducted only for AB4 and ES2 batches as shown in Figure 3.18. Major improvements up to 47% was observed in G_{IIC} values with respect to the reference composite material when 6 mg/m² SWCNT was introduced by electro spray deposition onto the twill woven CF fabric as summarized in Table 3.13. In the case of electro spray deposition; improvements in G_{IIC} values with respect to the reference decreased with further increase in the SWCNT amount incorporated. This can be attributed to the increasing amount of PVP between laminates, which may tend to ease sliding between tested laminates. Interestingly, the trend in ES2 batch did not match with air brush sprayed samples as shown in Figure 3.18-(a) and summarized in Table 3.12. The highest increase with 29% was observed for the 12 mg/m² SWCNT containing sample (AB4_400). Although 6 mg/m² and 18mg/m² ppm SWCNT containing samples still showed improvements compared to the control sample, they had relatively lower G_{IIC} values compared to sample containing 12mg/m² SWCNT.

Table 3.12 Mode-II Fracture Toughness Test Results of AB4 batch

Sample	G_{IIC}	Change
	(N/m)	(%)
AB4_REF	1637 ± 229	0
AB4_200	1836 ± 81	12.2
AB4_400	2115 ± 159	29.2
AB4_600	1967 ± 278	20.2

Table 3.13 Mode-II Fracture Toughness Test Results of ES2 batch

Sample	G_{IIC}	Change
	(N/m)	(%)
ES2_REF	1742 ± 415	0
ES2_200	2552 ± 367	46.5
ES2_400	2382 ± 344	36.8
ES2_600	2039 ± 75	17.1

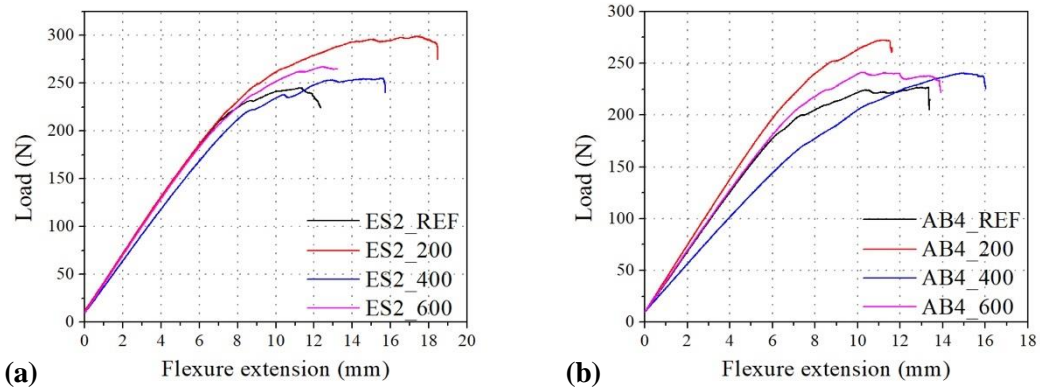


Figure 3.18 Load versus flexure extension graph, Mode-II fracture toughness test of (a) ES2, (b) AB4 batches

3.3.4. Three-Point Bending Test Results

Comparison of three-point bending test results for composite samples with and without SWCNTs showed that their addition led to slight change in flexural strength, modulus and strain values. AB1-H₂O and AB1_REF samples had similar flexural properties in AB1 batch, indicating that treating CF fabrics with a waterborne dispersion has no negative effects. According to the three-point bending test results in Table 3.14, only the flexural strength of AB1-0.1 sample has increased by 4.5%. However, there exists an increase in the flexural strain values of AB1-0.01 and AB1-0.1 samples by 9.5 % and 14.7%, respectively, which can be attributed to the crack bridging effect of SWCNTs. Since specimens of AB1 were manufactured with UD fabric, it is relatively difficult to observe the influence of SWCNTs on the flexural strength and modulus [23].

Table 3.14 Three-point bending test results of AB1 batch

Sample	Flexural Modulus	Flexural Strength	Flexural Strain
	(MPa)	(MPa)	(%)
AB1_REF	17468 ± 729	692 ± 30.58	3.93 ± 0.12
AB1-0.01	17474 ± 768	699 ± 25.80	4.3 ± 0.27
AB1-0.1	17187 ± 1639	722 ± 38.31	4.51 ± 0.15
AB1-H2O	17587 ± 73	694 ± 13.46	4.14 ± 0.19

The manufacturing process of AB2 batch was kept identical to AB1, yet the flexural values obtained from three-point bending tests of AB2 samples including the reference and samples containing same amount of SWCNTs presented abruptly different values except for flexural strength values as seen in Table 3.15. The reason behind such a difference could be attributed to varying fiber-resin content from AB1 to AB2 batch. Flexural results of AB2 series with increased resin content did not offer any improvements by incorporation of SWCNTs.

Table 3.15 Three-point bending test results of AB2 batch

Sample	Flexural Modulus	Flexural Strength	Flexural Strain
	(MPa)	(MPa)	(%)
AB2_REF	32705 ± 666	702 ± 26.00	2.14 ± 0.05
AB2-0.01	34672 ± 1641	710 ± 22.46	2.20 ± 0.07
AB2-0.01-2	34542 ± 615	661 ± 38.32	2.05 ± 0.04
AB2-0.02	33992 ± 613	692 ± 17.72	2.17 ± 0.02

In the case of ES1 batch, the incorporation of 50 ppm SWCNTs from a 0.01wt% SWCNT-H₂O dispersion (ES1-0.01) has shown the best improvement as seen in Table 3.16. Flexural modulus values increased by 9.4%, whereas flexural strength increased by 13.4% and flexural strain increased by 11%. The rest of the specimens manufactured in the same batch showed flexural properties in between the reference sample and ES1-0.01 sample.

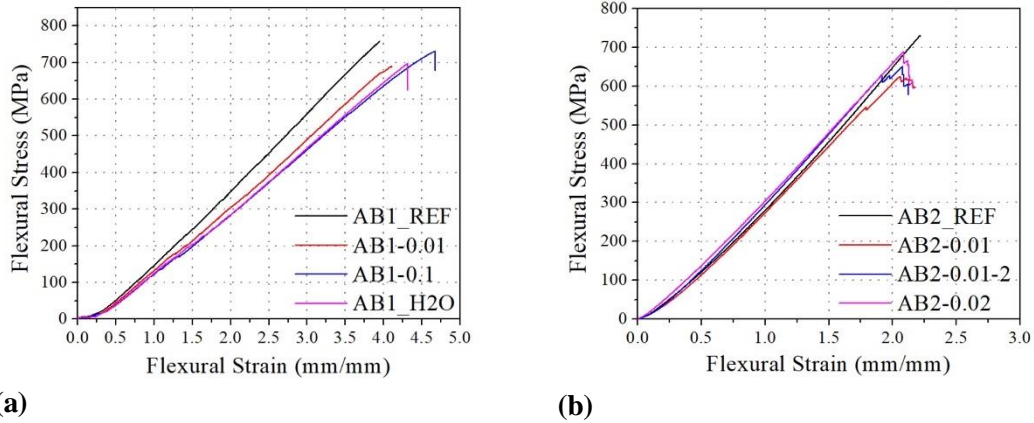


Figure 3.19 Flexural Stress versus flexural strain of (a) AB1 and (b) AB2 batches

Table 3.16. Three-point bending test results of ES1 batch

Sample	Flexural Modulus	Flexural Strength	Flexural Strain
	(MPa)	(MPa)	(%)
ES1_REF	41560 ± 901	663 ± 25.77	1.72 ± 0.09
ES1-0.005	41467 ± 149	706 ± 42.10	1.84 ± 0.18
ES1-0.01	45467 ± 126	752 ± 48.43	1.91 ± 0.05
ES1-0.02	43700 ± 213	688 ± 18.01	1.76 ± 0.04

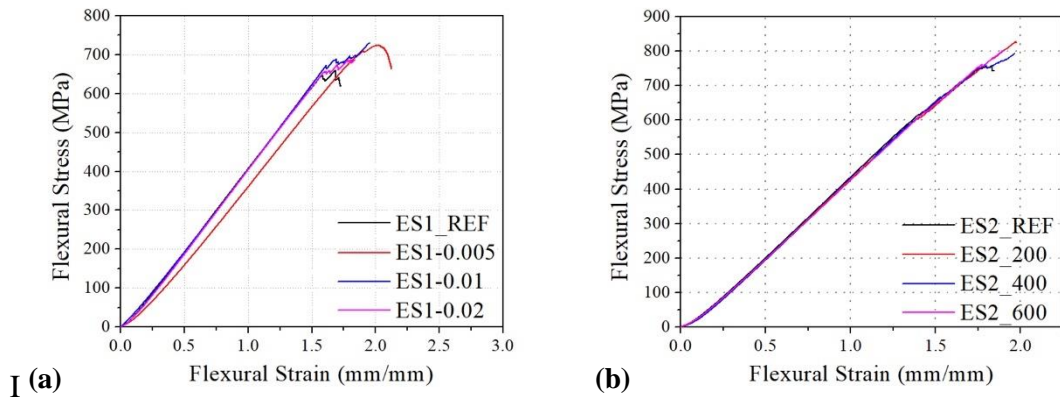


Figure 3.20 Flexural Stress versus flexural strain of (a) ES1 and (b) ES2 batches

The manufacturing process for ES2 and AB6 batches were kept analogous to each other to investigate the effect of SWCNT incorporation by two different methods. ES2 and AB6 were manufactured in two different vacuum bags; however, both ES2_REF and AB6_REF showed similar flexural values given in Tables 3.17 and 3.18, respectively, which allowed to make reliable comparisons between composite samples with different

SWCNT contents deposited by two methods. The highest improvement in flexural strength, 8.5% and 9.1% was seen in 30 ppm addition of SWCNT in air brush spray and electro spray deposition, respectively. As seen in flexural stress versus flexural strain graphs in Figure 3.20-(b) and 3.21, SWCNT incorporation higher than 30 ppm gradually decreased flexural strength values of composite samples in both batches.

Table 3.17 Three-point bending test results of ES2 batch

Sample	Flexural Modulus	Flexural Strength	Flexural Strain
	(MPa)	(MPa)	(%)
ES2_REF	47225 ± 310	752 ± 27.70	1.81 ± 0.04
ES2_200	46534 ± 289	821 ± 5.30	1.96 ± 0.02
ES2_400	47034 ± 209	792 ± 2.65	1.94 ± 0.04
ES2_600	46667 ± 306	805 ± 17.09	1.97 ± 0.05

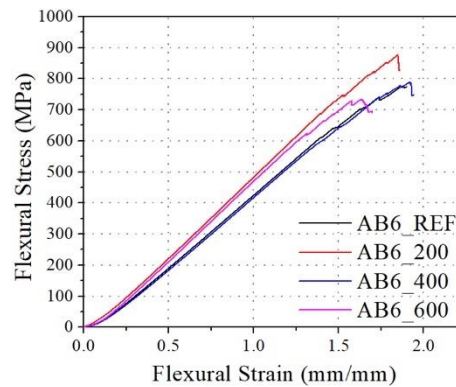


Figure 3.21 Flexural Stress versus flexural strain of AB6 batch

Table 3.18 Three-point bending test results of AB6 batches

Sample	Flexural Modulus	Flexural Strength	Flexural Strain
	(MPa)	(MPa)	(%)
AB6_REF	45575 ± 450	761 ± 44.38	1.86 ± 0.06
AB6_200	48900 ± 312	826 ± 44.65	2.01 ± 0.04
AB6_400	46734 ± 209	789 ± 8.00	1.94 ± 0.02
AB6_600	47200 ± 722	806 ± 2.65	1.93 ± 0.05

Flexural properties of ES/AB batch showed slightly lower degrees of improvements compared to AB6 and ES2 batches. In the ES/AB series, the effect of PVP alone on the flexural properties of the FRPCs was investigated by electro spraying PVP-H₂O containing solutions. The amount of PVP incorporated onto CF fabrics was kept identical to the amount of PVP introduced for the incorporation of 30, 60 and 90 ppm SWCNTs into FRPC structures. It should be noted that, the incorporation of PVP alone has only resulted in 2-3 % increase in flexural properties such as; flexural modulus, strength and strain. But increasing the amount of PVP further in the FRPC structure did not show any direct correlation with mechanical performance.

Similar to the trend observed in AB6 and ES2 batches, the highest flexural strength values were obtained with the incorporation of 30 ppm SWCNTs by both deposition methods in ES/AB batch. As summarized in Table 3.19, an improvement of 11.9% by electro spray (ES-CNT_200) and 12.2% by airbrush spray (AB-CNT_200) depositions were observed in flexural strength values with 30 ppm SWCNTs. In this batch, the incorporation of 5 ppm of SWCNT by depositing 1mg/m² SWCNT on each CFs surface was also evaluated (ES-CNT_30); however, no significant change was observed in flexural properties in comparison to ES/AB_REF sample.

Table 3.19 Three-point bending test results of ES/AB batch

Sample	Flexural Modulus	Flexural Strength	Flexure strain
	(MPa)	(MPa)	(%)
ES/AB_REF	44210 ± 409	738 ± 24.14	1.79 ± 0.07
ES-PVP_200	45740 ± 424	757 ± 8.54	1.78 ± 0.04
ES-PVP_400	45054 ± 324	762 ± 25.9	1.81 ± 0.04
ES-PVP_600	44630 ± 250	754 ± 11.33	1.84 ± 0.02
ES-CNT_30	43990 ± 134	731 ± 6.03	1.77 ± 0.03
ES-CNT_200	47648 ± 306	826 ± 17.38	1.88 ± 0.02
ES-CNT_400	45195 ± 503	770 ± 14.11	1.84 ± 0.04
ES-CNT_600	46970 ± 241	810 ± 7.59	1.87 ± 0.05
AB-CNT_30	40320 ± 521	736 ± 12.73	1.98 ± 0.04
AB-CNT_200	48395 ± 366	828 ± 9.54	1.85 ± 0.04
AB-CNT_400	46270 ± 241	764 ± 7.78	1.84 ± 0.03
AB-CNT_600	48137 ± 516	807 ± 22.04	1.85 ± 0.03

3.3.5. Short Beam Bending Test Results

The resistance of fabricated composite samples against delamination was measured by the short-beam shear test. The short beam bending tests for interlaminar shear strength and flexural strain measurements were executed only for FRPCs produced with electro spray coated fabrics in ES2 batch. The interlaminar shear strength of composite samples was found to increase linearly with respect to the overall SWCNT content in the composite structure as seen in Table 3.20 and Figure 3.22. ES2_200 sample has shown 4.8%, ES2_400 sample has shown %6.1 and ES2_600 has shown 8% increase in their interlaminar shear strength. Flexural strain at maximum load was enhanced by 6.7%, 11.1% and 8.5% for ES2_200, ES2_400 and ES2_600, respectively.

Table 3.20 Short beam shear test results of ES2 batch

Sample	ILSS	Flex. strain (ILSS)
	(MPa)	(%)
ES2_REF	63.84 ± 1.12	5.65 ± 0.09
ES2_200	66.94 ± 0.74	6.03 ± 0.05
ES2_400	67.74 ± 0.55	6.28 ± 0.06
ES2_600	68.90 ± 1.07	6.13 ± 0.08

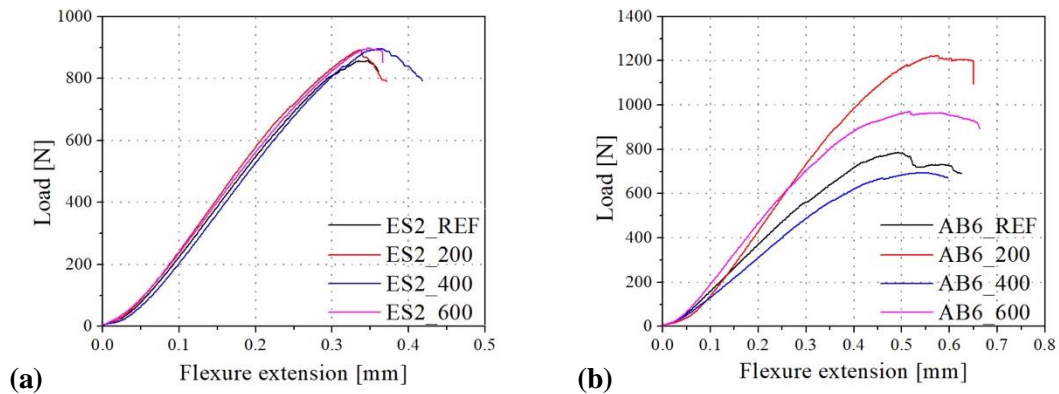


Figure 3.22 Load versus flexural extension, ILSS of (a) ES2 and (b) AB6 batches

AB6 batch prepared with airbrush sprayed CF fabrics was also tested for interlaminar shear. All samples in this batch showed similar improvements to each other in their interlaminar shear strength values with 4.7 %, 6 % and 5.6 % improvements for AB6_200, AB6_400 and AB6_600 samples, respectively as summarized in Table 3.21. When these values for AB6 batch in Table 3.21 was compared with interlaminar shear strength values

of ES2, they exhibit similar trends with increasing SWCNT content in the composite structure.

Table 3.21 Short beam shear test results of AB6 batch

Sample	ILSS	Flex. strain (ILSS)
	(MPa)	(%)
AB6_REF	63.81 ± 1.08	5.66 ± 0.19
AB6_200	66.83 ± 0.20	6.22 ± 0.22
AB6_400	67.61 ± 0.32	6.19 ± 0.08
AB6_600	67.37 ± 1.20	6.56 ± 0.25

3.3.6. V-Notched Shear Test Results

V-notched shear tests were performed on ES1, ES2 and AB6 batches. The incorporation of SWCNTs by airbrush spray and electrospray methods showed little or no effect on the shear properties of composite samples. Table 3.22, 3.23 and 3.24 summarize the V-notched shear test results of ES1, ES2 and AB6 batches, respectively. Figure 3.23 and 3.24 represent average compressive stress versus compressive strain graphs obtained from V-notched shear tests. SWCNT incorporation at various levels by neither electrospray nor airbrush spray deposition showed any significant effects on the V-notched shear properties of composite samples. In addition the shear properties of reference composite samples having no SWCNTs from ES2 and AB6 batches match each other very well, showing that the fabrication of ES2 and AB6 batches were analogous and the comparison of the mechanical test results from these two batches is reliable.

Table 3.22 Shear properties of ES1 batch

Sample	Shear Modulus	Shear Strength	Shear Strain	Offset Shear Strength
	(MPa)	(MPa)	(%)	(MPa)
ES1_REF	2409 ± 12	53.50 ± 0.59	22.75 ± 1.33	30.47 ± 0.16
ES1-0.005	2517 ± 18	54.90 ± 2.31	24.02 ± 0.07	31.96 ± 1.91
ES1-0.01	2639 ± 24	55.49 ± 1.19	23.74 ± 0.30	32.12 ± 0.58
ES1-0.02	2554 ± 92	55.75 ± 1.81	23.71 ± 0.47	31.39 ± 0.72

Table 3.23 Shear properties of ES2 batch

Sample	Shear Modulus	Shear Strength	Shear Strain	Offset Shear Strength
	(MPa)	(MPa)	(%)	(MPa)
ES2_REF	3016 ± 68	105.89 ± 12.49	22.65 ± 0.78	34.34 ± 0.77
ES2_200	3117 ± 12	105.45 ± 5.04	23.19 ± 0.79	36.10 ± 0.64
ES2_400	2966 ± 19	110.77 ± 2.42	23.87 ± 0.02	37.15 ± 0.83
ES2_600	3051 ± 14	108.18 ± 1.41	23.73 ± 0.11	35.00 ± 0.12

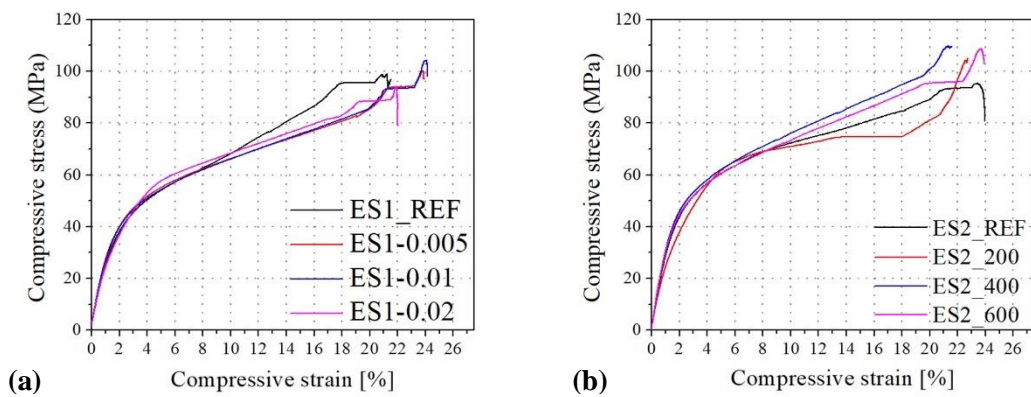


Figure 3.23 Compressive stress versus compressive strain graph of (a) ES1 and (b) ES2 batches obtained from V-notched method

Table 3.24 Shear properties of AB6

Sample	Shear Modulus	Shear Strength	Shear Strain	Offset Shear Strength
	(MPa)	(MPa)	(%)	(MPa)
AB6_REF	2859 ± 78	106.74 ± 4.41	23.76 ± 0.24	33.23 ± 0.64
AB6_200	2867 ± 11	110.36 ± 1.27	23.10 ± 0.80	33.23 ± 0.37
AB6_400	2928 ± 17	107.37 ± 1.30	23.87 ± 0.07	33.21 ± 0.29
AB6_600	3014 ± 10	102.21 ± 2.20	23.56 ± 0.13	33.52 ± 0.41

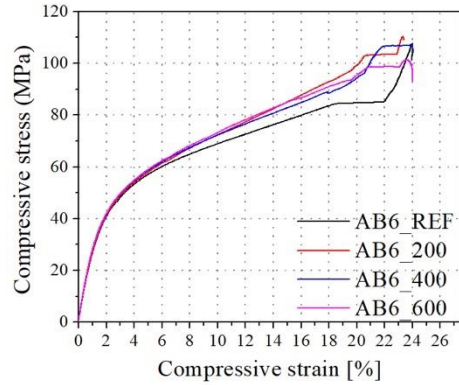


Figure 3.24 Compressive stress versus compressive strain graph of AB6 batch obtained from V-notched method

3.4. SEM Analysis of Fractured Surfaces

The analysis of fractured surfaces by SEM is an effective tool for the understanding of the effect of SWCNTs on the adhesion phenomena between the matrix and the resin. SEM images of FPRC specimens from ES2 batch tested under Mode-I fracture toughness test are shown in Figures 3.25 and 3.26. In the majority of analyzed fractured surfaces, the presence of numerous SWCNTs is evident after the resin infusion, composite curing and mechanical testing steps, which also indicates the presumed bridging and anchoring role of the SWCNTs at the polymer-fiber interface in FRPCs throughout this study.

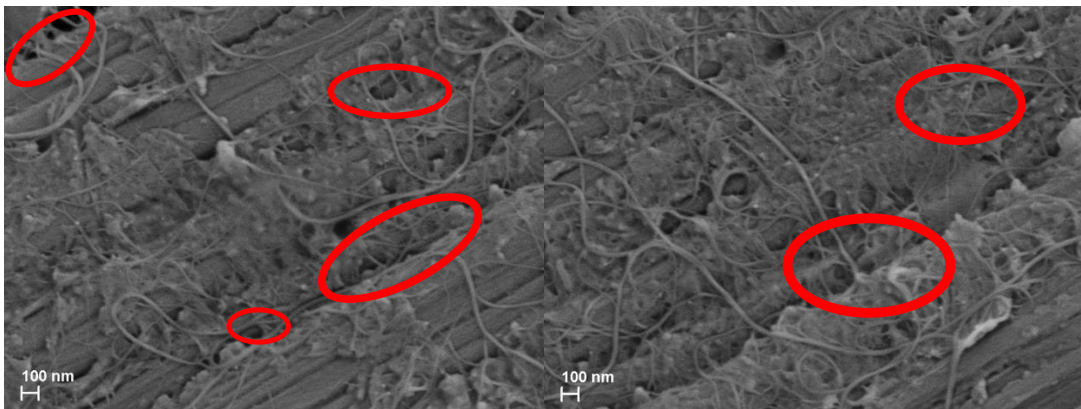


Figure 3.25 SEM images of fractured mode-I specimen ES2_200 sample

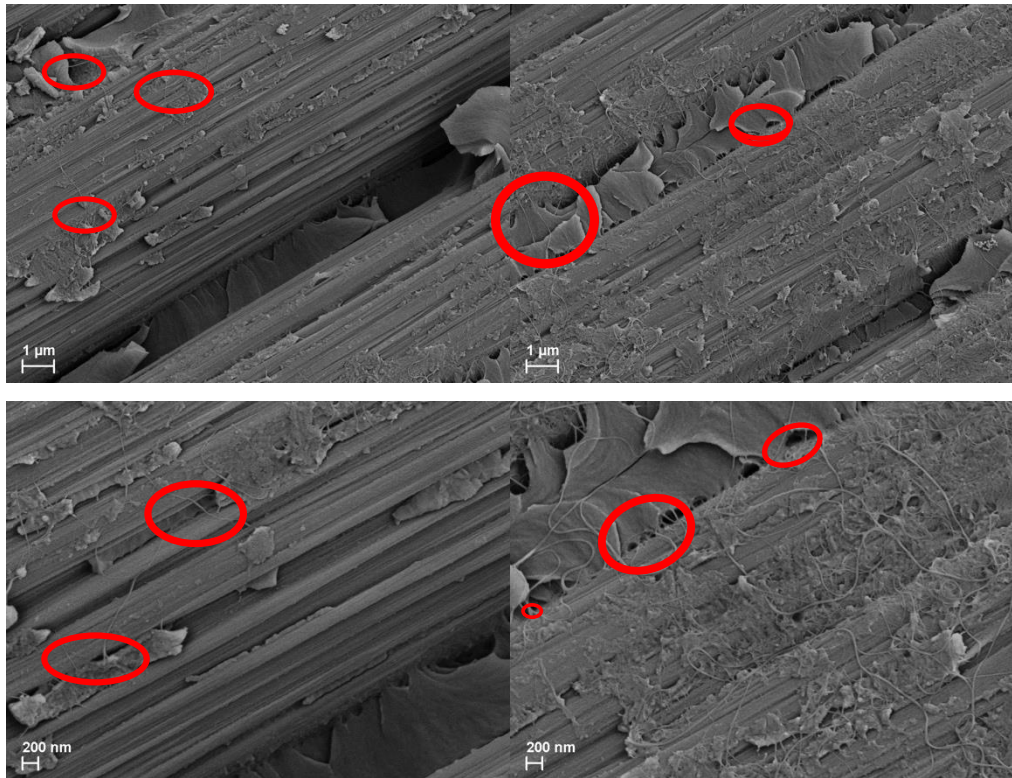


Figure 3.26 SEM images of SWCNT matrix-fiber bridging in ES2_200 sample

Chapter 4

CONCLUSIONS

This thesis presented the incorporation of SWCNTs into FRPCs from waterborne dispersions for the first time in the literature as an excellent candidate for tailoring interfacial properties of FRPCs to improve mechanical performance. Airbrush spray deposition and electrospray deposition of SWCNTs onto CF fabrics using waterborne dispersion of SWCNTs was demonstrated as an appropriate method to improve interfacial interactions of fiber and matrix. SEM images of fractured FRPC samples revealed that SWCNTs introduced on the CF fabric surface prior to the composite fabrication were richly present at the polymer-fiber interface after the composite fabrication by VIP and mechanical testing. This clearly proves that SWCNTs deposited on the CF fiber surface not only increase the surface area of reinforcing fibers but also impart additional interlocking bridges between fibers and the matrix, resulting in an enhanced stress transfer between them. Both methods have shown similar influence in the final composite properties including tensile, shear, fracture and flexural properties, yet the electrospray deposition of SWCNTs has resulted in a more homogeneous and fine distribution of SWCNTs in most cases.

The adhesion between the laminate plies was strengthened and fracture toughness was improved for FRPCs with SWCNT contents varying from as low as 30 to 90 ppm. For instance, the highest G_{IC} fracture toughness values up to 20% were obtained with electrospray deposition of 12 mg/m² SWCNTs on the CF surface whereas the airbrush spray deposition of 6 mg/m² SWCNTs resulted in similar improvements. On the other hand, G_{IIC} values of FRPCs manufactured with electrospray deposited CF fabrics containing 6 mg/m² SWCNTs had 46% improvement, whereas composite samples from the identical 12 mg/m² airbrush sprayed CF fabrics had 29% improvement, showing an

opposite trend to G_{IC} improvements with respect to the overall SWCNT content in the composite structure.

Tensile and interlaminar shear tests have shown similar results with the incorporation of 60 ppm SWCNTs in the composite structure with both electrospray and airbrush spray deposition methods; however, maximum value of flexural properties up to 12% improvement was observed with 30 ppm SWCNT incorporation by both methods.

Higher amount of SWCNT incorporation into the overall composite, 90 ppm, with deposition of 18 mg/m² SWCNTs on each surface didn't result in any promising mechanical performances during any of the mechanical tests. In addition, the incorporation of SWCNTs did not show any improvements on the shear properties of composites.

Tensile and flexural properties of composite structures containing only PVP at the polymer-fiber interface were also determined, which showed no significant effect, demonstrating that main contribution to the improvement of mechanical performance of the composite structures arise from the presence of SWCNT on the fiber-matrix interface. Overall mechanical test results showed that an optimum SWCNT content would be required for the highest property improvement depending on the type of CF fabric used, the deposition method and the type of desired property improvement.

It can also be stated that electrospray deposition of SWCNTs is more practical and beneficial compared to airbrush spray deposition method and 30-60 ppm SWCNTs in the overall composite structure is the optimum amount for FRPCs fabricated in this study.

REFERENCES

- [1] Zhao Z, Teng K, Li N, Li X, Xu Z, Chen L, Niu J, Fu H, Zhao L and Liu Y 2017 Mechanical, thermal and interfacial performances of carbon fiber reinforced composites flavored by carbon nanotube in matrix/interface *Compos. Struct.* **159** 761–72
- [2] Li M, Gu Y, Liu Y, Li Y and Zhang Z 2013 Interfacial improvement of carbon fiber/epoxy composites using a simple process for depositing commercially functionalized carbon nanotubes on the fibers *Carbon N. Y.*
- [3] Campbell F C 2010 Structural Composite *Struct. Compos. Mater.* 31–61
- [4] Garg M, Sharma S and Mehta R 2015 Pristine and amino functionalized carbon nanotubes reinforced glass fiber epoxy composites *Compos. Part A Appl. Sci. Manuf.* **76** 92–101
- [5] Iijima S 1991 Helical microtubules of graphitic carbon *Nature* **354** 56–8
- [6] Radushkevich L V. and Lykhanovich V M 1952 O strukture ugleroda, obrazujucesojja pri termiceskom razlozenii okisi ugleroda na zeleznom kontakte *Zhurnal Fiz. Khimii*
- [7] Avilés F, de Jesús Kú-Herrera J and Oliva-Avilés A I 2017 Deposition of carbon nanotubes on fibers *Carbon Nanotube-Reinforced Polymers: From Nanoscale to Macroscale* (Elsevier Inc.) pp 117–44
- [8] Lin T, Bajpai V, Ji T and Dai L 2003 Chemistry of carbon nanotubes *Aust. J. Chem.* **56** 635–51
- [9] Naidu P K, Pulagara N V and Dondapati R S 2014 Carbon Nanotubes in Engineering Applications: A Review *Prog. Nanotechnol. Nanomater.* **3** 79–82
- [10] Ajayan P M 1999 Nanotubes from Carbon *Chem. Rev.* **99** 1787–800
- [11] Dai H 2002 Carbon nanotubes: Synthesis, integration, and properties *Acc. Chem. Res.* **35** 1035–44
- [12] Siddiqui N, Li C, Ma P and Kim J 2009 Carbon Nanotubes with Dual Wall Structure; Properties and Fracture Behavior of Epoxy Nanocomposites *17th Int. Conf. Compos. Mater.* 1–12
- [13] Hu L, Hecht D S and Grüner G 2010 Carbon Nanotube Thin Films: Fabrication, Properties, and Applications *Chem. Rev.* **110** 5790–844
- [14] Britto P J, Santhanam K S V., Rubio A, Alonso J A and Ajayan P M 1999

- Improved Charge Transfer at Carbon Nanotube Electrodes *Adv. Mater.* **11** 154–7
- [15] Che G, Lakshmi B B, Fisher E R and Martin C R 1998 Carbon nanotubule membranes for electrochemical energy storage and production *Nature* **393** 346–9
- [16] Davis D C, Wilkerson J W, Zhu J and Hadjiev V G 2011 A strategy for improving mechanical properties of a fiber reinforced epoxy composite using functionalized carbon nanotubes *Compos. Sci. Technol.* **71** 1089–97
- [17] Garcia E J, Wardle B L, John Hart A and Yamamoto N 2008 Fabrication and multifunctional properties of a hybrid laminate with aligned carbon nanotubes grown In Situ *Compos. Sci. Technol.* **68** 2034–41
- [18] Sharma M, Gao S, Mäder E, Sharma H, Wei L Y and Bijwe J 2014 Carbon fiber surfaces and composite interphases *Compos. Sci. Technol.* **102** 35–50
- [19] De Riccardis M F, Carbone D, Makris T D, Giorgi R, Lisi N and Salernitano E 2006 Anchorage of carbon nanotubes grown on carbon fibres *Carbon N. Y.* **44** 671–4
- [20] Qian H, Greenhalgh E S, Shaffer M S P and Bismarck A 2010 Carbon nanotube-based hierarchical composites: A review *J. Mater. Chem.* **20** 4751–62
- [21] Zhang Z, Pfefferle L and Haller G L 2015 Characterization of functional groups on oxidized multi-wall carbon nanotubes by potentiometric titration *Catal. Today* **249** 23–9
- [22] García E J, Hart A J and Wardle B L 2008 Long Carbon Nanotubes Grown on the Surface of Fibers for Hybrid Composites *AIAA J.* **46** 1405–12
- [23] Che J and Chan-Park M B 2008 Reactive spinning of cyanate ester fibers reinforced with aligned amino-functionalized single wall carbon nanotubes *Adv. Funct. Mater.* **18** 888–97
- [24] Haji A, Rahbar R S and Shoushtari A M 2015 Plasma assisted attachment of functionalized carbon nanotubes on poly(ethylene terephthalate) fabric to improve the electrical conductivity *Polimery/Polymers* **60** 337–42
- [25] Islam M S, Deng Y, Tong L, Faisal S N, Roy A K, Minett A I and Gomes V G 2016 Grafting carbon nanotubes directly onto carbon fibers for superior mechanical stability: Towards next generation aerospace composites and energy storage applications *Carbon N. Y.* **96** 701–10
- [26] Che J, Yuan W, Jiang G, Dai J, Lim S Y and Chan-Park M B 2009 Epoxy composite fibers reinforced with aligned single-walled carbon nanotubes functionalized with generation 0-2 dendritic poly(amidoamine) *Chem. Mater.* **21**

- [27] Sager R J, Klein P J, Lagoudas D C, Zhang Q, Liu J, Dai L and Baur J W 2009 Effect of carbon nanotubes on the interfacial shear strength of T650 carbon fiber in an epoxy matrix *Compos. Sci. Technol.* **69** 898–904
- [28] He X, Wang C, Tong L, Wang R, Cao A, Peng Q, Moody S and Li Y 2012 Direct measurement of grafting strength between an individual carbon nanotube and a carbon fiber *Carbon N. Y.* **50** 3782–8
- [29] An F, Lu C, Guo J, He S, Lu H and Yang Y 2011 Preparation of vertically aligned carbon nanotube arrays grown onto carbon fiber fabric and evaluating its wettability on effect of composite *Appl. Surf. Sci.* **258** 1069–76
- [30] Wang C, Li Y, Tong L, Song Q, Li K, Li J, Peng Q, He X, Wang R, Jiao W and Du S 2014 The role of grafting force and surface wettability in interfacial enhancement of carbon nanotube/carbon fiber hierarchical composites *Carbon N. Y.* **69** 239–46
- [31] Pozegic T R, Anguita J V., Hamerton I, Jayawardena K D G I, Chen J S, Stolojan V, Balocchi P, Walsh R and Silva S R P 2016 Multi-Functional Carbon Fibre Composites using Carbon Nanotubes as an Alternative to Polymer Sizing *Sci. Rep.* **6** 1–11
- [32] Carley G, Geraldo V, Oliveira S de and Avila A F 2013 Nano-engineered composites: interlayer carbon nanotubes effect *Mater. Res.* **16** 628–34
- [33] Wicks S S, Wang W, Williams M R and Wardle B L 2014 Multi-scale interlaminar fracture mechanisms in woven composite laminates reinforced with aligned carbon nanotubes *Compos. Sci. Technol.* **100** 128–35
- [34] Wicks S S, de Villoria R G and Wardle B L 2010 Interlaminar and intralaminar reinforcement of composite laminates with aligned carbon nanotubes *Compos. Sci. Technol.* **70** 20–8
- [35] Kepple K L, Sanborn G P, Lacasse P A, Gruenberg K M and Ready W J 2008 Improved fracture toughness of carbon fiber composite functionalized with multi walled carbon nanotubes *Carbon N. Y.* **46** 2026–33
- [36] Madou M J 2006 *Fundamentals of Microfabrication, The Science of Miniaturization, Second Edition*
- [37] Armitage N P, Gabriel J C P and Grüner G 2004 Quasi-Langmuir-Blodgett thin film deposition of carbon nanotubes *J. Appl. Phys.* **95** 3228–30
- [38] Dan B, Irvin G C and Pasquali M 2009 Continuous and scalable fabrication of

transparent conducting carbon nanotube films *ACS Nano*

- [39] Mujika F, Vargas G, Ibarretxe J, De Gracia J and Arrese A 2012 Influence of the modification with MWCNT on the interlaminar fracture properties of long carbon fiber composites *Compos. Part B Eng.* **43** 1336–40
- [40] Zhang H, Liu Y, Kuwata M, Bilotti E and Peijs T 2015 Improved fracture toughness and integrated damage sensing capability by spray coated CNTs on carbon fibre prepreg *Compos. Part A Appl. Sci. Manuf.* **70** 102–10
- [41] Chaudhry M S, Czekanski A and Zhu Z H 2017 Characterization of carbon nanotube enhanced interlaminar fracture toughness of woven carbon fiber reinforced polymer composites *Int. J. Mech. Sci.* **131–132** 480–9
- [42] Almuhammadi K, Alfano M, Yang Y and Lubineau G 2014 Analysis of interlaminar fracture toughness and damage mechanisms in composite laminates reinforced with sprayed multi-walled carbon nanotubes *Mater. Des.* **53** 921–7
- [43] Garcia E J, Wardle B L and John Hart A 2008 Joining prepreg composite interfaces with aligned carbon nanotubes *Compos. Part A Appl. Sci. Manuf.* **39** 1065–70
- [44] Deng C, Jiang J, Liu F, Fang L, Wang J, Li D and Wu J 2015 Influence of Carbon Nanotube Coatings on Carbon Fiber by Ultrasonically Assisted Electrophoretic Deposition on Its Composite Interfacial Property *Surf. Coatings Technol.* **272** 176–81
- [45] Tamrakar S, An Q, Thostenson E T, Rider A N, Haque B Z and Gillespie J W 2016 Tailoring Interfacial Properties by Controlling Carbon Nanotube Coating Thickness on Glass Fibers Using Electrophoretic Deposition *ACS Appl. Mater. Interfaces* **8** 1501–10
- [46] Dimitrios Tasis,^{*},[†] Nikos Tagmatarchis,[‡] Alberto Bianco and M P 2003 Chemistry of carbon nanotubes *Aust. J. Chem.* **56** 635–51
- [47] Rodriguez A J, Guzman M E, Lim C S and Minaie B 2011 Mechanical properties of carbon nanofiber/fiber-reinforced hierarchical polymer composites manufactured with multiscale-reinforcement fabrics *Carbon N. Y.* **49** 937–48
- [48] Bekyarova E, Thostenson E T, Yu A, Kim H, Gao J, Tang J, Hahn H T, Chou T-W, Itkis M E and Haddon R C 2007 Multiscale carbon nanotube-carbon fiber reinforcement for advanced epoxy composites. *Langmuir* **23** 3970–4
- [49] Maulik S, Sarkar A, Basu S and Daniels-Race T 2018 Voltage-Controlled Spray Deposition of Multiwalled Carbon Nanotubes on Semiconducting and Insulating

- Substrates *J. Electron. Mater.* **47** 4604–9
- [50] Li Q, Church J S, Naebe M and Fox B L 2016 A systematic investigation into a novel method for preparing carbon fibre–carbon nanotube hybrid structures *Compos. Part A Appl. Sci. Manuf.* **90** 174–85
- [51] Seemann L, Stemmer A and Naujoks N 2007 Local surface charges direct the deposition of carbon nanotubes and fullerenes into nanoscale patterns *Nano Lett.* **7** 3007–12
- [52] Lee C W, Raman Pillai S K, Luan X, Wang Y, Li C M and Chan-Park M B 2012 High-performance inkjet printed carbon nanotube thin film transistors with high-k hfo₂ dielectric on plastic substrate *Small*
- [53] Denneulin A, Bras J, Blayo A, Khelifi B, Roussel-Dherbey F and Neuman C 2009 The influence of carbon nanotubes in inkjet printing of conductive polymer suspensions *Nanotechnology*
- [54] Song J W, Kim J, Yoon Y H, Choi B S, Kim J H and Han C S 2008 Inkjet printing of single-walled carbon nanotubes and electrical characterization of the line pattern *Nanotechnology*
- [55] Jo J W, Jung J W, Lee J U and Jo W H 2010 Fabrication of highly conductive and transparent thin films from single-walled carbon nanotubes using a new non-ionic surfactant via spin coating *ACS Nano*
- [56] ASTM International 2000 ASTM D 3039/D 3039M ASTM Standard Test Method for Tensile Properties of Polymer Matrix Composite Materials *Annu. B. ASTM Stand.* **15.03** 105–16
- [57] Standard(DIN-EN 6033) 2015 Aerospace series - Carbon fiber reinforced plastics - Test method - Determination of interlaminar fracture toughness energy - Mode I - GIC *Dtsch. Inst. Fur Normung*
- [58] Prasad M S S, Venkatesha C S and Jayaraju T 2011 Experimental Methods of Determining Fracture Toughness of Fiber Reinforced Polymer Composites under Various Loading Conditions *J. Miner. Mater. Charact. Eng.* **10** 1263–75
- [59] Sadeghian R, Gangireddy S, Minaie B and Hsiao K 2005 Manufacturing carbon nanofibers toughened polyester / glass fiber composites using vacuum assisted resin transfer molding for enhancing the mode-I delamination resistance **37** 1787–95
- [60] Standard(DIN-EN 6034) 2015 Aerospace series - Carbon fiber reinforced plastics - Test method - Determination of interlaminar fracture toughness energy - Mode II

- GIIC *Dtsch. Inst. Fur Normung*

- [61] ASTM International 2003 ASTM D 790-17 Standard Test Methods for Flexural Properties of Unreinforced and Reinforced Plastics and Electrical Insulating Materials 1 *Annu. B. ASTM Stand.* 11
- [62] ASTM International 2003 ASTM D 2344/D 2344M: Standard Test Method for Short-Beam Strength of Polymer Matrix Composite Materials and Their Laminates *Annu. B. ASTM Stand.* **3** 136–40
- [63] ASTM International 2012 ASTM D 5379/D 5379M Standard Test Method for Shear Properties of Composite Materials by the V-Notched *Annu. B. ASTM Stand.* 1–13
- [64] Rayleigh, Lord and Lord Rayleigh 1882 On the Equilibrium of Liquid Conducting Masses charged with Electricity *Philos. Mag. Ser. 5* **14** 184–6
- [65] Monfared Zanjani J S, Okan B S, Menciloglu Y Z and Yildiz M 2016 Nano-engineered design and manufacturing of high-performance epoxy matrix composites with carbon fiber/selectively integrated graphene as multi-scale reinforcements *RSC Adv.* **6** 9495–506
- [66] O’Shea J N, Taylor J B, Swarbrick J C, Magnano G, Mayor L C and Schulte K 2007 Electrospray deposition of carbon nanotubes in vacuum *Nanotechnology* **18**